# Shear & Ellipticity in Gravitational Lenses

C.R. Keeton

C.S. Kochanek

U. Seljak
Harvard-Smithsonian Center for Astrophysics, MS-51
60 Garden Street
Cambridge MA 02138

## ABSTRACT

Galaxies modeled as singular isothermal ellipsoids with an axis ratio distribution similar to the observed axis ratio distribution of E and S0 galaxies are statistically consistent with both the observed numbers of two-image and four-image lenses and the inferred ellipticities of individual lenses. However, no four-image lens is well fit by the model (typical $\chi^2/N_{dof} \sim 20$), the axis ratio of the model can be significantly different from that of the observed lens galaxy, and the major axes of the model and the galaxy may be slightly misaligned. We found that models with a second, independent, external shear axis could fit the data well (typical $\chi^2/N_{dof} \sim 1$), while adding the same number of extra parameters to the radial mass distribution does not produce such a dramatic improvement in the fit. An independent shear axis can be produced by misalignments between the luminous galaxy and its dark matter halo, or by external shear perturbations due to galaxies and clusters correlated with the primary lens or along the line of sight. We estimate that the external shear perturbations have no significant effect on the expected numbers of two-image and four-image lenses, but that they can be important perturbations in individual lens models. However, the amplitudes of the external shears required to produce the good fits are larger than our estimates for typical external shear perturbations (10-15% shear instead of 1-3% shear) suggesting that the origin of the extra angular structure must be intrinsic to the primary lens galaxy in most cases.

*Subject headings:* gravitational lensing – cosmology – galaxies: elliptical and lenticular

## 1. Introduction

We generally think of dark matter in galaxies in the context of the radial distribution of mass. Galaxy rotation curves for spirals, and X-ray halos (e.g. Fabbiano 1995) and gravitational lensing (Maoz & Rix 1993, Kochanek 1995, 1996a) for early type galaxies all require radial mass distributions that decline more slowly than the luminosity. Stellar dynamical models of early-type galaxies can generally be made consistent with dark matter either present or absent depending on the assumptions about the structure of the stellar orbits (Saglia et al. 1993, Carollo et al. 1995). However, once we accept that the radial mass distribution is substantially composed of dark matter, there is little basis for believing that the ellipticity of the luminous matter is quantitatively representative of the ellipticity of the overall mass distribution. In spiral galaxies we accept this premise as a matter of course – the light distribution is a flattened disk, but the dark matter distribution is a moderately oblate spheroid.

The shapes of early-type galaxies are a mixture of oblate, prolate, and triaxial spheroids, although the inferred shape distributions (e.g. Schechter (1987), Ryden (1992), Jørgensen & Franx (1994)) are limited by the degeneracies inherent in deprojection (e.g. Rybicki 1987) and by triaxiality. Kinematic misalignments between the projected angular momentum vector and the minor axis of the projected galaxy provide clear geometric evidence that the intrinsic shapes of ellipticals are triaxial (Binney 1985, Franx et al. 1991). The observed axis ratios of the combined E & S0 population show a deficit of round galaxies, a plateau for axis ratios from 0.9 to 0.6, and a sharp decline beyond 0.5. Observational evidence on the shape of the mass distribution in early type galaxies is very limited. Models of the rare polar-ring galaxies (e.g. Arnaboldi & Sparke 1994, Sackett et al. 1994) give inferred density axis ratios of $0.3 \lesssim c/a \lesssim 0.6$, similar or flatter than the inferred axis ratios of the central galaxy. Buote & Canizares (1994, 1995, 1996) studied the ellipticity of the X-ray halos of several elliptical galaxies. In NGC 720 they found that the dark matter had $0.3 \lesssim c/a \lesssim 0.5$, and in NGC 1332 they found $0.2 \lesssim c/a \lesssim 0.7$, and the dark matter was at least as flattened as the luminous galaxy. In NGC 720, the projected major axes of the dark and luminous matter were misaligned by $30^\circ \pm 15^\circ$ (90% confidence). Theoretical models of galaxy formation predict ellipticities and triaxialities for the mass distribution larger than observed for luminous galaxies (Dubinski 1992, 1994, Warren et al. 1992). Although the calculations contained only dark matter, some differences between the dark matter and the baryons should persist as a consequence of the different dissipative processes in dark matter and gas.

Gravitational lenses are sensitive to the angular structure of the projected mass distribution of the lens galaxies through both the distributions of image morphologies

(two-image, four-image etc.) and detailed models of individual lenses. We already know from circular models of lenses that the radial mass distribution of successful lens models is inconsistent with constant mass-to-light ratio dynamical models both from statistical studies (Maoz & Rix 1993, Kochanek 1993, 1996a) and models of individual lenses (e.g. Kochanek 1995, Grogin & Narayan 1996). Gravitational lenses supply three probes of the angular structure. The first is the ellipticity required to produce the observed numbers of two-image and four-image lenses. The second is the ellipticity required to fit particular lensed systems, and the third is the alignment of the inferred mass distribution with the observed lens galaxy. If galaxies contain dark matter, then the ellipticities of the light distributions need not match those of the mass distributions, and if the dark matter distribution has either a different triaxiality than the luminous distribution or is not in dynamical equilibrium, the models need not be aligned with the observed galaxy. The numerical models of halo formation predict that the mass distributions should be both more elliptical and more triaxial than the light distribution.

Statistical models using non-circular lenses (Kochanek & Blandford 1987, Kochanek 1991b, Wallington & Narayan 1993, Kassiola & Kovner 1993) focused on the existence of detectable numbers of bright four-image quasar lenses as a consequence of magnification bias, and they did not quantitatively evaluate the ellipticities required to fit the observed distribution of lens morphologies. More recently, King et al. (1996) pointed out that the models used in these studies clearly produce fewer four-image lenses than are observed in the JVAS radio lens survey (Patnaik 1994, Patnaik et al. 1992). Kochanek (1996b) quantified the mismatch in greater detail for both the JVAS survey and optical quasar lens surveys. Models of individual lenses strongly constrain the lens ellipticity for a given radial mass distribution, with centrally concentrated distributions requiring higher ellipticities than extended, dark matter distributions (see Kochanek 1991a, Wambsganss & Paczyński 1994). Except for these preliminary surveys, there are no systematic comparisons of the angular properties of lens models to the expected properties of galaxies.

There is, however, a complication to any program using lenses to study the angular structures of galaxies – the primary lens galaxy is not the only source of shear in a gravitational lens. The most important sources of external shears are galaxies or clusters correlated with the primary lens galaxy (Kochanek & Apostolakis 1988), galaxies or clusters near the line of sight but at a different redshift (Kochanek & Apostolakis 1988, Jaroszyński 1991) and perturbations from large scale structure (Gunn 1967, Jaroszyński et al. 1990, Jaroszyński 1991, Seljak 1994, Bar-Kana 1996). Strong external perturbations are rare, with only two lenses clearly requiring multiple components in the lens model. The lens 0957+561 (Walsh, Carswell & Weymann 1980) is a composite consisting of a galaxy and a cluster (Young et al. (1980), most recently modeled by Grogin & Narayan 1996), and

the lens 2016+112 (Lawrence et al. 1984) has two lens galaxies that may be at different redshifts (e.g. Nair & Garrett 1996). Weak external shear perturbations can also be probed by observing the correlations of galaxy ellipticities (e.g. Blandford et al. 1991, Miralda-Escudé 1991, Kaiser 1992) or by measuring the weak shear produced by individual galaxies (e.g. Valdes et al. 1984, Brainerd et al. 1996).

In our analysis we will quantitatively survey the origins of ellipticity and shear, the numbers of lenses of different morphologies, and models of the individual lenses and compare the results to the optical properties of early type galaxies. In §2 we review the sources of shear in gravitational lenses: the primary lens galaxy, objects clustered with the lens galaxy, objects near the ray path, and shear from large scales structures. In §3 we briefly summarize the lens data we use in our analysis, and our analytical procedures. In §4 we consider the case of lensing by isolated early-type galaxies. In §5 we study the effects of adding additional sources of shear to the lens model. Finally, in §6 we review our results.

## 2. The Sources Of Shear In Gravitational Lenses

The ellipticity and shear in a gravitational lens comes from three sources: the primary lens galaxy, galaxies or clusters near the lens galaxy, and structures along the ray path. The primary galaxy is characterized by its ellipticity or axis ratio, and all external perturbations can be characterized by their external shear $\gamma$. The structures along the ray path range from weak potential fluctuations to galaxies and clusters. We first define the general gravitational lensing equations needed to describe our models, and then discuss each of the sources of ellipticity and shear.

We are interested in the case where there is already a strong lens, and the effects of weak shear perturbations are to modify the lens equations into a "generalized quadrupole lens" (Kovner 1987). Relative to a fiducial ray passing from the observer through the lens center in the absence of the lens potential, the lens equation, following the notation of Bar-Kana (1996), is

$$\vec{u} = (I + F_{OS})\vec{x} - (I + F_{LS})\vec{\alpha}\,[(I + F_{OL})\vec{x}] \tag{1}$$

where $\vec{u}$ is the angular position of the source compared to the fiducial ray, $\vec{x}$ is the angular position in the lens plane compared to the fiducial ray, $\vec{\alpha}$ is the deflection produced by the primary lens galaxy, and $I$ is the $2 \times 2$ identity matrix. The $2 \times 2$ tensors $F_{OS}$, $F_{OL}$, and $F_{LS}$ describe additional shear and convergence due to perturbations between the observer and the source, the observer and the lens, and the lens and the source respectively. Each tensor can be decomposed into a convergence $\kappa$, a shear $\gamma$, and orientation of the major axis of the shear $\theta$, where $\kappa = (1/2)(F_{11} + F_{22})$, $\gamma_c = \gamma \cos 2\theta = (1/2)(F_{11} - F_{22})$,

$\gamma_s = \gamma \sin 2\theta = F_{12} = F_{21}$, and $\gamma^2 = \gamma_c^2 + \gamma_s^2$.

Statistical calculations are simplified by using the "equivalent plane" defined by the coordinates $\vec{X} = (1 + F_{OL})\vec{x}$ and $\vec{U} = (1 + F_{LS})^{-1}\vec{u}$ (Kovner 1987). The lens equation in the equivalent plane is

$$\vec{U} = (I - F_e)\vec{X} - \vec{\alpha}(\vec{X}). \tag{2}$$

In these coordinates, and to linear order, the effects of the three shear tensors reduce to a single effective shear and convergence tensor, $F_e = F_{OL} + F_{LS} - F_{OS}$, added to the effects of the primary lens (Bar-Kana 1996). The advantage of the effective plane is that cross sections and magnification probability distributions depend only on $F_e$ in the effective plane but are easily transformed back into the normal coordinates. If $\sigma'$ is a cross section computed in the equivalent plane, then the cross section in the original coordinates is $\sigma'|I + F_{LS}|^{-1}$, and if $M'$ is a magnification computed in the equivalent plane, then the magnification in the original coordinates is $M^{-1} = (M')^{-1}|I + F_{LS}||I + F_{OL}|$, where $|\cdots|$ denotes a determinant. If the convergence and shear of $F$ are $\kappa$ and $\gamma$, then $|I + F| = (1 - \kappa)^2 - \gamma^2$. If we only use cross sections and magnifications computed in the effective plane, we make errors in the statistical calculation that are first order in $\kappa$ (second order if $\langle\kappa\rangle = 0$ as in the LSS model of §2.3) and second order in $\gamma$.

### 2.1. The Primary Lens Galaxy

The primary lens galaxy in most lens systems is an early type galaxy (E or S0), with only 10–20% of lenses contributed by spiral galaxies (Fukugita & Turner 1991, Maoz & Rix 1993, Kochanek 1996). Given the general mass uncertainties for galaxies, we can lump the E and S0 galaxies into a common population for the purposes of lens models. For simplicity the calculations will neglect the effects of misalignments between the luminous galaxy and the dark matter halo, although we consider whether the problems in the model can be explained by these effects. Although we are assuming a dark matter model, we would like to compare our inferences to the observed axis ratios of luminous galaxies. We used the Jørgensen & Franx (1994) sample of 53 E and 93 S0 galaxies in the Coma cluster to estimate the axis ratio distribution of E and S0 galaxies. The natural ellipticity parameter for lens models is the eccentricity $\epsilon$, where the two-dimensional axis ratio is $q_2^2 = (1 - \epsilon)/(1 + \epsilon)$. We modeled the eccentricity distribution with a Gaussian, $dP/d\epsilon \propto \exp(-(\epsilon - \epsilon_0)^2/2\Delta\epsilon_0^2)$ $(0 \le \epsilon \le 1)$, and the peak Kolmogorov-Smirnov (K–S) test probability for fitting the joint E+S0 distribution was 94% for parameters of $\epsilon_0 = 0.26$ and $\Delta\epsilon_0 = 0.33$. The E galaxies have lower mean ellipticities (peak of 82% for $\epsilon_0 = 0.14$ and $\Delta\epsilon_0 = 0.15$) than the S0 galaxies (peak of 94% for $\epsilon_0 = 0.44$ and $\Delta\epsilon_0 = 0.21$). The mean ellipticity of the ellipticals

is underestimated because many low ellipticity S0 galaxies are misclassified as ellipticals (see Jørgensen & Franx 1994). If the ellipticity of the light is a guide to the ellipticity of the mass, high ellipticity lens galaxies are S0 galaxies and low ellipticity lens galaxies are ellipticals.

We limited our study to a single model for the primary lens galaxy, the singular isothermal ellipsoid. We chose the model because singular isothermal spheres (SIS) are the only models known to be simultaneously consistent with gravitational lens statistics, models, and stellar dynamics (see Kochanek 1996a). We consider other monopole structures in Keeton & Kochanek (1996b). The singular isothermal ellipsoid was used by Kassiola & Kovner (1993) to study the statistics of lensed quasars and by Kormann et al. (1994a) to model B 1422+231. Kassiola & Kovner (1993) and Kormann et al. (1994b) discuss the model's analytic properties in detail. The projected surface density of the singular isothermal ellipsoid is

$$2\frac{\Sigma}{\Sigma_c} = \frac{b}{r}\frac{\eta(\epsilon)}{(1-\epsilon\cos 2\theta)^{1/2}} \tag{3}$$

where $\Sigma_c = c^2(1+z_l)D_{OS}/4\pi G D_{OL} D_{LS}$ is the critical surface density for gravitational lensing, and $b = 4\pi(\sigma/c)^2 D_{LS}/D_{OS}$ is the tangential critical radius of the circular SIS for a one-dimensional dark matter velocity dispersion of $\sigma$ normalized to match the observed line-of-sight velocity dispersions $\langle v_{los}^2\rangle$ of galaxies (see Kochanek 1994). We use only an $\Omega_0 = 1$ cosmological model, where the comoving distances are $D_{ij} = 2r_H((1+z_i)^{-1/2} - (1+z_j)^{-1/2})$ for $r_H = c/H_0$. For $z_i = 0$, $D_{ij}$ is the proper motion distance to $z_j$. The factor $\eta(\epsilon)$ is an ellipticity dependent normalization factor, and $\eta(\epsilon = 0) \equiv 1$.

Lens calculations are normalized to group lenses with fixed line-of-sight stellar velocity dispersions, $\langle v_{los}^2\rangle^{1/2}$, so the normalization factor $\eta(\epsilon)$ should be defined so that $\langle v_{los}^2\rangle$ is fixed as we vary $\epsilon$. The stellar dynamics of ellipsoidal stellar distributions in ellipsoidal dark matter distributions is a little studied problem (e.g. de Bruijne, van der Marel & de Zeeuw 1996), and a detailed examination is well beyond the scope of our study. To gain a qualitative understanding of $\eta$, we consider the idealized problem in which both the luminosity and density distributions are axisymmetric, oblate ($0 < q_3 < 1$) singular isothermal ellipsoids with density

$$\rho = \frac{\sigma_0^2}{2\pi G}\frac{1}{R^2 + z^2/q_3^2}. \tag{4}$$

and projected surface density

$$\Sigma = \frac{\sigma_0^2(1+\epsilon)q_3}{2GR(1-\epsilon\cos 2\theta)^{1/2}} \quad \text{where} \quad \epsilon = \frac{2(1-q_3^2)\sin^2 i}{3+q_3^2+(1-q_3^2)\cos 2i}, \tag{5}$$

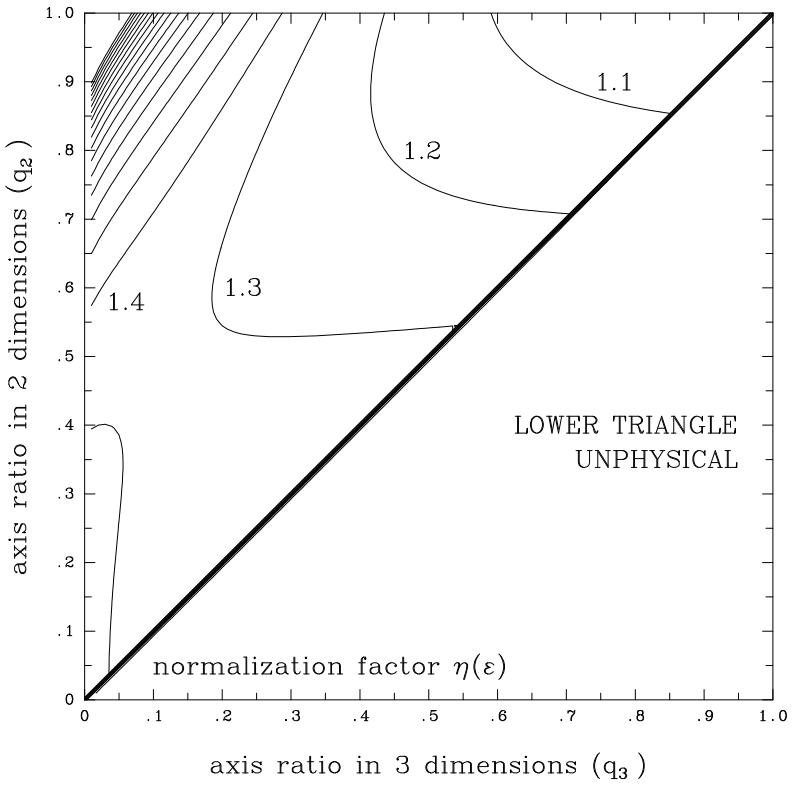


Fig. 1.— The normalization factor $\eta$ for isothermal ellipsoids with three-dimensional axis ratio $q_3$ and two-dimensional axis ratio $q_2$. Only the upper-left triangle is physical because $q_2 \geq q_3$. Contours are spaced every 0.1 from $\eta = 1$ for a spherical system to $\eta = 3$ for nearly pole-on ($q_2 \sim 1$) flattened systems ($q_3 \sim 0$).

and $i$ is the inclination angle of the galaxy relative to the observer ($i = 0$ is pole on). The velocity $\sigma_0$ is an unmeasurable parameter that must be related to the line-of-sight velocity dispersion of the stars, $\langle v_{los}^2 \rangle$, through the normalization factor $\eta = \sigma_0^2(1+\epsilon)q_3/\langle v_{los}^2 \rangle$.

We can determine the velocity dispersions of the isothermal ellipsoid analytically for an axisymmetric two-integral dynamical model (Binney & Tremaine 1987, §4.2) assuming a constant mass-to-light ratio with stellar density $\nu = \rho$. The velocity dispersions in the cylindrical $R$ and $Z$ directions are equal with

$$\nu\sigma_R^2 = \nu\sigma_Z^2 = \frac{\nu_0\sigma_0^2}{R^2a^2}\left[\left(\tan^{-1}a\right)^2 - \left(\tan^{-1}a|x|\right)^2\right] \tag{6}$$

where $a^2 = e^2/(1-e^2)$, $e^2 = 1 - q_3^2$, and $r$ and $x = \cos\theta$ are spherical polar coordinates. The mean square velocity in the direction of the cylindrical angle $\phi$ is

$$\nu\langle v_\phi^2 \rangle = \frac{2\sigma_0^2\nu_0 \tan^{-1}a}{r^2a(1+a^2x^2)} - \nu\sigma_R^2. \tag{7}$$

For fixed $\sigma_0$ in eqn. (4), adding ellipticity reduces the stellar velocity dispersions relative to the spherical model at all positions in the galaxy. The line-of-sight velocity dispersion through an infinite aperture can be reduced to a simple one-dimensional integral,

$$\frac{\langle v_{los}^2 \rangle}{\sigma_0^2} = \sin^2 i \frac{\tan^{-1}a}{a} + \cos^2 i \int_0^{\pi/2} dx \frac{\left(\tan^{-1}a\right)^2 - \left(\tan^{-1}ax\right)^2}{a(1-x^2)\tan^{-1}a}. \tag{8}$$

Figure 1 shows contours of $\eta$ as a function of the two- and three-dimensional axis ratios of the ellipsoid. In general, the lensing surface density in eqn. (3) with $\eta = 1$ underestimates lensing by flattened galaxies for a fixed line-of-sight velocity dispersion at all inclination angles. Edge-on, modestly flattened galaxies ($q_3 > 1/2$, $q_2 \sim q_3$) produce more lenses than pole-on or rounder galaxies, so the normalization factor enhances the number of lenses produced by the more elliptical lenses (e.g. Subramanian & Cowling 1986). We will use $\eta = 1$ for the lensing calculations, because our dynamical model is not quantitatively accurate. With $\eta = 1$ we underestimate the numbers of lenses produced by high ellipticity galaxies, causing us to overestimate the numbers of high ellipticity galaxies required to fit the data by $\eta^2(\epsilon)$.

### 2.2. Galaxies and Clusters Near the Primary Lens

The galaxy correlation function enhances the probability of finding another galaxy near the primary lens, and it is more likely that a perturbing galaxy is at the redshift of the primary lens galaxy than elsewhere along the line of sight (see Kochanek & Apostolakis

1988). Early type galaxies also tend to live in high-density environments (e.g. Postman & Geller 1984), further increasing the probability of finding a nearby perturbing galaxy. We consider the shear produced by the nearest neighbor galaxy, and the shear produced by clusters of galaxies. The shear from perturbers at the same redshift as the primary lens have $F_{OS}$ non-zero, and $F_{LS} \equiv 0$ and $F_{OL} \equiv 0$ in the generalized quadrupole lens of eqn. (1).

In three dimensions, the galaxy-galaxy correlation function is $\xi(r) = (r/r_0)^{-\chi}$ where the comoving correlation length is $r_0 \simeq 5h^{-1}$ Mpc and the exponent is $\chi \simeq 1.75$ (e.g. Peebles 1995). We model the shear from a neighbor by $\gamma = \gamma_{bk}(2a/r - 1)$ for $r < a$ and $\gamma_{bk}a^2/r^2$ for $r > a$ where $\gamma_{bk} = b/4a$ is the shear at the break radius $a \sim$ 50–200 kpc. For $r < a$ the model becomes an SIS lens, while for $r > a$ it is a point mass lens. If $\gamma > \gamma_{max} = 2b/r_{min} \simeq 1/4$, then the two lenses have interacting caustics and the perturbation cannot be modeled by a shear tensor (see Kochanek & Apostolakis 1988). The optical depth for the nearest neighbor to produce a shear exceeding $\gamma$ is

$$\tau(>\gamma) \simeq 0.01 \left[\frac{n_*}{10^{-2}h^3\ \mathrm{Mpc}^{-3}}\right] \left[\frac{(1+z_l)r_0}{5h^{-1}\mathrm{Mpc}}\right]^{7/4} \left[\frac{\sigma_*}{220\ \mathrm{km\ s}^{-1}}\right]^{5/2} \left[\frac{D_{OS}}{r_H}\right]^{5/4} x^{5/4}(1-x)^{5/4}\gamma^{-5/4}. \tag{9}$$

for $\chi = 1.75$, and a constant comoving density of lenses $n_*$ with a Schechter (1976) function exponent $\alpha = -1$ and a "Faber-Jackson" exponent $\gamma_{FJ} = 4$ (see §3), where $x = D_{OL}/D_{OS}$ is the fractional distance of the primary lens from the observer. The ratio $D_{OS}/r_H = 1$ at $z_s \simeq 3$ for an $\Omega_0 = 1$ cosmological model. The peak shear perturbation is found at $x = 1/2$, the optimal distance for the primary lens, where the optical depth reaches $\tau(>\gamma) \simeq 0.002(D_{OS}/r_H)^{5/4}\gamma^{-5/4}$. These expressions fail when the optical depth approaches unity (typically at impact parameters smaller than $a$, which allows us to ignore the regime $r > a$). We can approximate the minimum shear scale by truncating the optical depth at $\tau(>\gamma_{min}) = 1$, where $\gamma_{min} \simeq 0.025x(1-x)(D_{OS}/r_H) \lesssim 0.005(D_{OS}/r_H)$. The optical depth for non-linear interactions between galaxies is

$$\tau(\gamma > \gamma_{max} \simeq 1/4) \simeq 0.06x^{5/4}(1-x)^{5/4}\left(\frac{D_{OS}}{r_H}\right)^{5/4} \lesssim 0.01\left(\frac{D_{OS}}{r_H}\right)^{5/4} \tag{10}$$

so lenses with more than one primary lens galaxy are rare (as observed).

The opposite limit to considering only the nearest neighbor galaxy is to put the primary lens galaxy in a cluster. The local comoving density of clusters as a function of velocity dispersion $\sigma$ is approximately $dn/d\sigma \simeq (n_0/\sigma_0)(\sigma/\sigma_0)^{-c}$ with $c \simeq 8.4 \pm 1.0$, $n_0 = 3.6^{+1.6}_{-1.0} \times 10^{-3}h^3$ Mpc$^{-3}$ and $\sigma_0 = 400$ km s$^{-1}$ using Henry & Arnauld's (1991) X-ray luminosity function and assuming $\sigma^2 = kT/\mu m_p$ ($\beta \simeq 1$) to relate the velocity dispersion $\sigma$ to the X-ray temperature $T$. Let the cluster mass distribution be an SIS

truncated at outer radius $r_c$ where $r_c = r_{c0}(\sigma/\sigma_0)^y$, and the galaxy distribution in the cluster be $n_g(r_g/r)^2$ with the same outer radius. The cluster shear is $\gamma = b/2r$ where $b = b_0(\sigma/\sigma_0)^2$, $b_0 = 4\pi(\sigma_0/c)^2 D_{LS}/D_{OS}$, the shear at the cluster edge is $\gamma_{min} = \gamma_0(\sigma/\sigma_0)^{2-y}$, and $\gamma_0 = b_0/2r_{c0}$. The shear probability distribution is convergent and dominated by the low mass clusters if $c > 3 + y$. We now consider only the self-similar solution with $y = 2$ for which the shear distribution is independent of the cluster velocity dispersion. The integral optical depth is

$$\begin{aligned} \tau(>\gamma) &= \frac{8\pi^2}{c-5} n_0 r_H [(1+z_l) r_{c0}]^2 \left(\frac{\sigma_0}{c}\right)^2 \frac{D_{OS}}{r_H} \frac{x(1-x)}{\gamma} \\ &= 0.01 \left[\frac{n_0}{4\times 10^{-3} h^3 \mathrm{Mpc}^{-3}}\right] \left[\frac{(1+z_l) r_{c0}}{5 h^{-1} \mathrm{Mpc}}\right]^2 \left[\frac{\sigma_0}{400 \beta^{1/2} \text{ km s}^{-1}}\right]^2 \frac{D_{OS}}{r_H} \frac{x(1-x)}{\gamma} \end{aligned} \quad (11)$$

assuming a constant comoving density of clusters truncated at $\sigma_0$. Thus if every lens galaxy is in a cluster, the shear contribution from the clusters is nearly equal to the shear from the nearest neighbor galaxies (eqn. 10). However, by assuming a constant comoving density of clusters, eqn. (12) significantly overestimates the contribution from clusters, so we expect that the shear distribution is dominated by the nearest neighbor galaxies.

*The cluster shear contribution is dominated by the groups and small clusters with a negligible contribution from large clusters.* Since the fraction of the optical depth from clusters with velocity dispersions exceeding $\sigma$ is $(\sigma/\sigma_0)^{-3.4\pm1.0}$, half of the optical depth is from velocity dispersions within 20% of the lower limit (between $\sigma_0$ and $1.2\sigma_0$). In the observed lens sample it is clear that large clusters are unimportant because lensing by rich clusters is found only by looking at rich clusters as part of surveys for arcs (see Kneib & Soucail 1996). The only convincing cluster-scale lens found by searching for lensed sources (i.e. not selected based on the mass of the lens) is 0957+561 (Walsh et al. 1979, Young et al. 1980), where the cluster is exactly the type of poor, sparse cluster expected to dominate the statistics. The convergence produced by a cluster is tightly correlated with the shear ($\kappa = \gamma$ for the SIS model), so the optical depth for large convergences is also small. Previous models of multiply imaged quasars considered the extra convergence produced by clusters, but not the extra shear (e.g. Turner, Ostriker, & Gott 1984, Maoz & Rix 1993, Kochanek 1993). Since large shear perturbations are easily detected, it is unlikely that cluster convergences can be significantly distorting gravitational lens statistics.

### 2.3. Perturbations Along the Line-of-Sight: Large Scale Structure

We next consider the shear generated by weak, long-wavelength inhomogeneities along the line of sight, which we will refer to as large scale structure (LSS) shear, following the

approach of Bar-Kana (1996) based on earlier studies by Gunn (1967), Kovner (1987), Kaiser (1992) and Seljak (1994, 1996). Light propagating through the universe is deflected by inhomogeneities along the line of sight. Although the total deflection angle can be of the order of arcminutes, the relative distortion of a bundle of photons is small. Such weak lensing does not generate multiple images, but it does distort the shapes of background sources. The distortions may be measurable from the ellipticities of high redshift galaxies (e.g. Blandford et al. 1991; Miralda-Escudé 1991; Kaiser 1992).

Potential fluctuations between the observer and the primary lens produce $F_{OS}$ and $F_{OL}$ shear terms in the generalized quadrupole lens (eqn. (1)), while potential fluctuations between the primary lens and the source produce $F_{OS}$ and $F_{LS}$ terms. The $F_{LS}$ term is observable only in the lens time delays, so we focus on the effective shear $F_e = F_{OL} + F_{LS} - F_{OS}$ and the $F_{OL}$ shear. If we assume linear evolution of the power spectrum in an $\Omega_0 = 1$ universe, then the power spectrum of the potential fluctuations, $P_\phi(k,z) = 9\Omega^2 H^4 a^4 \Delta^2(k)/16\pi k^7$, is independent of redshift, and ensemble averages of the LSS shear terms depend only on

$$G = r_H^3 \int_0^\infty k^5 dk P_\phi(k) = \frac{\Omega_0^2 \sigma_R^2}{16\pi r_H k_0} \frac{\int_0^\infty dq q^{n+1} T^2(q)}{\int_0^\infty dq q^{n+2} T^2(q) [\sin(u) - u\cos(u)]^2/u^6}. \qquad (12)$$

The power spectrum is defined by $\Delta^2(k) = A k^{n+3} T_k(k)^2$ where $A$ is a normalization constant, $k^n$ is the primordial spectrum ($n \simeq 1$),

$$T_k = \frac{\ln(1+2.34q)}{q} \left[1 + 3.89q + (14.1q)^2 + (5.46q)^3 + (6.71q)^4\right]^{-1/4} \qquad (13)$$

is the BBKS (Bardeen et al. 1986) transfer function where $q = k/k_0$ and $k_0 = \Omega_0 h^2$ Mpc$^{-1}$, $u = Rk = Rk_0 q$, and the mean square density fluctuation in a top-hat filter of radius $R$ is

$$\sigma_R^2 = \int_0^\infty \Delta^2(k) \frac{dk}{k} \frac{9}{(kR)^6} \left(\sin kR - kR\cos kR\right)^2 . \qquad (14)$$

For $\Omega_0 h = 0.25$ and $n = 1$, we find $G = 1.2 \times 10^{-4} \sigma_8^2 h^{-1}$. Eqn. (13) is strictly valid only for $\Omega_0 = 1$ and linear evolution, but the results found using non-linear power spectrum models (Jain, Mo & White (1995), Peacock & Dodds (1996)) are relatively accurate (10–20% errors) over a wide range of $\Omega_0$ and $\lambda_0$. While the gravitational potential in $\Omega_0 < 1$ models decays in a linear model, the non-linear evolution and the longer path-lengths nearly cancel the decay so that eqn. (13) is roughly correct for other cosmological models.

The mean square effective shear, OL shear, and their correlation are determined by the weighted average over the potential $G$ and geometry. We find that

$$\langle \gamma_e^2 \rangle \;=\; \frac{4\pi^2}{5} G \left(\frac{D_{OS}}{r_H}\right)^3 x^2 (1-x)^2$$

$$\begin{aligned} \langle \gamma_{OL}^2 \rangle &= \frac{2\pi^2}{15} G \left( \frac{D_{OS}}{r_H} \right)^3 x^3 \\ \langle \gamma_{OL} \gamma_e \rangle &= -\frac{\pi^2}{5} G \left( \frac{D_{OS}}{r_H} \right)^3 x^3 (1-x). \end{aligned} \tag{15}$$

The maximum effective shear $\gamma_{em}^2 = (\pi^2 G/20)(D_{OS}/r_H)^3$ is found for a primary lens at one-half the distance to the source $x = D_{OL}/D_{OS} = 1/2$ and it scales with the source distance as $D_{OS}^{3/2}$ (Bar-Kana 1996). The deformation of the lens plane $\gamma_{OL}$ is determined by the $F_{OL}$ matrix, and it is strongest for a primary lens near the source. The $\gamma_e$ and $\gamma_{OL}$ shears are weakly anti-correlated, with a mean angle $\Delta\theta$ between them of $\langle \cos \Delta\theta \rangle = -(3x/8)^{1/2}$. We can more usefully characterize the average properties of the LSS shear by averaging over the lens cross section. For a SIS lens in a flat cosmology the differential optical depth is $d\tau \propto D_{OL}^2 D_{LS}^2 dD_{OL}$, and the cross section averaged shears are $\langle \gamma_e^2 \rangle = (16/21)\gamma_{em}^2$, $\langle \gamma_{OL}^2 \rangle = (10/21)\gamma_{em}^2$ and $\langle \cos \Delta\theta \rangle = -(5/32)^{1/2}$.

Figure 2 summarizes the strength of the LSS shear including the effects of non-linear power-spectra, the cosmological model, and $\sigma_8$. In the linear case the maximum rms LSS shear $\gamma_{em}$ is only 1–2% for $\sigma_8 \simeq 0.5$ (Eke et al. 1996) and a source at $z_s \sim 3$. The dominant contribution comes from Mpc scales, corresponding to the outer parts of clusters and to superclusters. In the non-linear case, the maximum rms shear is 4–6% and the dominant contribution comes from linear scales near $k^{-1} \sim 100$ kpc. In all models the strength of the LSS shear increases with $\sigma_8$ and $\Omega_0 h$.

### 2.4. Perturbations Along the Line-of-Sight: Nonlinear Objects

The LSS shear contribution is dominated by non-linear structures, and the linear scale of $k^{-1} \sim 100$ kpc dominating the shear in the non-linear power spectrum corresponds to a non-linear scale near $k^{-1} \sim 20$ kpc. Hence the shear in the non-linear power spectrum estimates is not caused by "large scale structure," but is an approximation to the shear produced by collapsed halos. Shear from galaxies along the line of sight was considered by Kochanek & Apostolakis (1988), Jaroszynski (1991) and it is related to the efforts by Valdes et al. (1984) and Brainerd et al. (1996) to measure weak shears produced by individual galaxies. In this subsection we develop the effects of discrete halos near the line of sight using the language of the LSS shear calculation.

A single perturber of the primary lens produces $F_{OS}$ and $F_{OL}$ shear terms if it is in the foreground and $F_{OS}$ and $F_{LS}$ shear terms if it is in the background. For a lens at fractional distance $x = D_{OL}/D_{OS}$ to the source, the integral optical depth for $\gamma_e$ using an

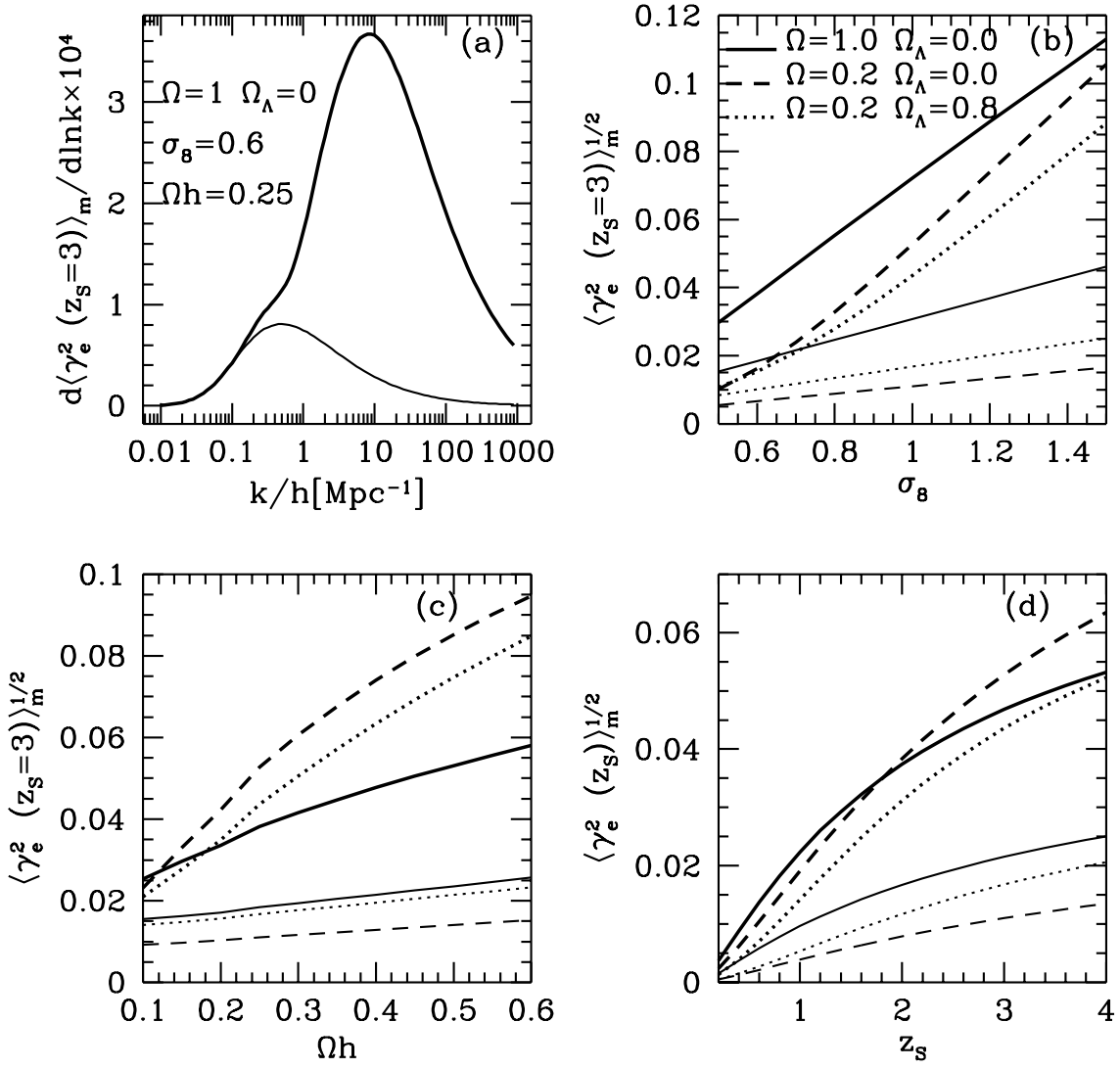


Fig. 2.— The dependence of LSS shear on cosmology for both linear (light) and non-linear (dark) power spectrum models. Panel (a) shows the logarithmic contribution to $\gamma_m(z_S = 3)$ as a function of wavevector $k$ for linear (light solid) and non-linear (heavy solid) power spectrum models. Panel (b) shows the dependence of $\gamma_m(z_S = 3)$ on the amplitude $\sigma_8$ for a fixed shape $\Omega_0 h = 0.25$. Panel (c) shows the dependence on the shape $\Omega_0 h$ for fixed amplitude, with $\sigma_8 = 0.6$ for $\Omega_0 = 1$ and $\sigma_8 = 1.0$ for $\Omega_0 < 1$. Finally, panel (d) shows the variation of the shear with source redshift for the models in panel (c) fixed to $\Omega_0 h = 0.25$.

SIS perturber model is

$$\begin{aligned}\tau(>\gamma_e) &= \frac{4}{5}\pi^3 n_* r_H^3 \left(\frac{\sigma_*}{c}\right)^4 \left(\frac{D_{OS}}{r_H}\right)^3 \frac{x^2(1-x)^2}{\gamma_e^2} \\ &= 0.002 \left[\frac{n_*}{10^{-2}h^3\ \mathrm{Mpc}^{-3}}\right] \left[\frac{\sigma_*}{220\ \mathrm{km\ s}^{-1}}\right]^4 \left(\frac{D_{OS}}{r_H}\right)^3 \frac{x^2(1-x)^2}{\gamma_e^2} \end{aligned} \quad (16)$$

and the integral optical depth for $\gamma_{OL}$ is

$$\tau(>\gamma_{OL}) = \frac{2}{15}\pi^3 n_* r_H^3 \left(\frac{\sigma_*}{c}\right)^4 \left(\frac{D_{OS}}{r_H}\right)^3 \frac{x^3}{\gamma_{OL}^2}. \quad (17)$$

We can truncate the distribution either at the point where the universe becomes optically thick, or at the value of the shear at the characteristic radius $a$ where the galaxy mass distribution begins to decline faster than the isothermal profile. Generally these scales are similar. Comparing the optical depth for $\gamma_e$ to the optical depth for correlated galaxies (eqn. (10)), we find that the correlated term is the more important for shears larger than $\gamma \gtrsim 0.12x(1-x)(D_{OS}/r_H)^{7/3} = 0.03(D_{OS}/r_H)^{7/3}$ for $x = 1/2$. The optical depths in eqns. (16) and (17) have the same distance scalings as the LSS shear results in eqn. (15), so we can define an effective $G$ parameter (eqn. (12)) by

$$G = 2\pi n_* r_H^3 \left(\frac{\sigma_*}{c}\right)^4 \ln\Lambda \simeq 5\times 10^{-4} \left[\frac{n_*}{10^{-2}h^3\ \mathrm{Mpc}^{-3}}\right] \left[\frac{\sigma_*}{220\ \mathrm{km\ s}^{-1}}\right]^4 \ln\Lambda. \quad (18)$$

The "Coulomb logarithm" is $\ln\Lambda = \ln(\gamma_{max}/\gamma_{min}) \simeq 3.2$, where $\gamma_{max} \simeq 0.25$ is the shear at which the caustics merge, and $\gamma_{min} \sim 0.01$ is the shear at which the universe becomes optically thick. The magnitude of $G$ calculated using discrete non-linear potentials qualitatively agrees with that calculated using the non-linear power spectrum in the LSS model ($G \simeq 3\times 10^{-4}$).

For weak shears the description in terms of discrete galaxies must fail because the universe is optically thick, so the true probability distribution for weak shears should approach the form expected for Gaussian random fields, $d\tau/d\gamma_e \propto \gamma_e \exp(-\gamma_e^2/\langle\gamma_e^2\rangle)$. For strong shears, the universe is optically thin, and the distribution must approach the discrete galaxy result, $d\tau/d\gamma_e \propto \gamma_e^{-3}$. We explored how the two limits merge using Monte Carlo simulations of lensing by a constant comoving density of Poisson-distributed galaxies. As expected, for $\gamma_e \gtrsim 0.1$ the shear is entirely due to the nearest galaxy and has the power law distribution, while for $\gamma_e \lesssim 0.02$ it is due to random combinations of weak shears from many galaxies and the distribution approaches the Gaussian limit. In the intermediate range, there is usually a dominant perturbing galaxy, but the effects of other nearby galaxies cannot be neglected.

Since large shear perturbations are dominated by a particular galaxy near the line of sight, we can estimate its properties. The mean distance to a $\gamma_e$ perturber is the distance to the primary lens, $D_{OL}$, while the mean distance to a $\gamma_{OL}$ perturber is one-half the distance to the primary lens, $D_{OL}/2$. The typical angular separation of a $\gamma_e$ perturber from the primary lens is $\simeq 0\farcs25/\gamma_e$, while the typical $\gamma_{OL}$ perturber is further away in angle, $\simeq 0\farcs37/\gamma_{OL}$, because it is physically closer to the observer. A $\gamma_{OL}$ perturber is generally brighter than the primary lens galaxy, both because it is closer to the observer and because it is rarely ideally placed as a lens (forcing it to be a more massive galaxy), while a $\gamma_e$ perturber is generally of comparable brightness to the primary lens galaxy. Finally, we can estimate the non-linearity of the perturber, or the fractional importance of the next order terms in the expansion of the perturber's gravitational field beyond the shear tensor. For $\gamma_e$ perturbers the non-linearity is of order $2\gamma_e\Delta\theta$ where $\Delta\theta$ is the diameter of the image system of the lens in arcseconds. The $\gamma_{OL}$ perturbers are generally more non-linear, with an average non-linearity of $6\gamma_{OL}\Delta\theta$. For a $\gamma_{OL} = 0.05$ perturbation of a $\Delta\theta = 2''$ lens, the next order terms have 64% of the strength of the linear shear terms.

## 3. Lens Data and Calculation Methods

We confine our analysis to gravitational lenses in well-defined samples for which we can make both models of the lenses and statistical models of the number of two- and four-image lenses. We use the the data from the quasar surveys (Maoz et al. 1993ab, Crampton et al. 1992 Yee et al. 1993, Surdej et al. 1993, Kochanek, Falco & Schild 1995) and the JVAS radio survey (Patnaik 1994, Patnaik et al. 1992, King et al. 1996). We do not include serendipitously discovered lenses, the MIT-Greenbank (MG, Burke et al. 1992) or the CLASS survey (Jackson et al. 1995, Myers et al. 1995, Myers 1996) lenses primarily because we cannot make statistical models of the numbers of lenses in these surveys.

We use the quasar lens sample used by Kochanek (1996a). The sample contains three two-image lenses (0142–100, LBQS 1009–0252 and 1208–1011) and two four-image lenses (PG 1115+080, and H 1413+117). We use the compact source subsample of the JVAS radio survey which contains two two-image lenses (B 0218+357 and a second double) and two four-image lenses (B 1422+231 and MG 0414+0534). We exclude B 1938+666 both because it has an extended source, which invalidates our statistical models, and because it has never been modeled. Table 1 lists the lenses we discuss and their properties. Keeton & Kochanek (1996a) provides a more extensive summary of the data, and we will discuss detailed models in Keeton & Kochanek (1996b).

Singular isothermal ellipsoids in an external shear generically produce 2, 3, 4, and

Table 1: Lens Data

| Lens | $z_s$ | $z_l$ | $N_{im}$ | $q_l$ | P.A. |
|---|---|---|---|---|---|
| PG 1115+080 | 1.72 | 0.29 | 4 | | |
| H 1413+117 | 2.55 | | 4 | | |
| MG 0414+0534 | 2.64 | | 4 | $0.80 \pm 0.02$ | $71° \pm 5°$ |
| B 1422+231 | 3.62 | | 4 | $0.73 \pm 0.13$ | $121° \pm 15°$ |
| 0142–100 | 2.72 | 0.49 | 2 | $0.71 \pm 0.05$ | $73° \pm 5°$ |
| B 0218+357 | (0.96) | 0.68 | 2 | | |

Notes – The source and lens redshifts are $z_l$ and $z_s$ respectively. The number of images is $N_{im}$. The axis ratio $q_l$ and position angle of the major axis (P.A.) are given with their uncertainties if known. The ellipticities and position angles are from Falco et al. (1996) for MG 0414+0534, Impey et al. (1996) for B 1422+231, and Falco et al. (1996) for 0142–100.

6 image systems depending on the amplitudes and relative orientations of the shears. The only systems we see are the two-image and four-image morphologies (with another image trapped and demagnified in the singular core). The three-image cusp morphology is produced by an exposed cusp caustic and consists of three images offset to one side of the lens galaxy (see Wallington & Narayan 1993 or Kassiola & Kovner 1993 for diagrams of the image geometries), and the six-image morphology is a four-image system near a cusp with two of the images associated with the cusp split into double images. The three-image cusp morphology is associated with large shears or ellipticities (or large core radii for non-singular lenses, see Kassiola & Kovner 1993), and the six-image morphologies are associated with nearly perpendicular shears and ellipticities.

A circular SIS lens has a total multiple imaging cross section of $\pi b^2$, and one simplification afforded by the model is that all cross sections consist of the circular cross section multiplied by a dimensionless function of the shear and ellipticity. To compute the magnification bias we need the cross section as a function of magnification, not just the total cross section. Let $\sigma_n(> M, f, b, \epsilon, \gamma, \Delta\theta)$ be the integral cross section for a lens with parameters $b$, $\epsilon$, $\gamma$, and $\Delta\theta$ to produce a total magnification greater than $M$ subject to some limit on the flux ratios of the images $f$. Because of the scaling of the SIS lens, we can write $\sigma_n(> M, f, b, \epsilon, \gamma, \Delta\theta) = \pi b^2 \hat{\sigma}_n(> M, f, \epsilon, \gamma, \Delta\theta)$ where $\hat{\sigma}_n$ does not depend on the mass scale of the lens $b$. In most cases we will average over the relative orientations of the two shear terms, and the angle averaged cross section is specified by $\sigma_n(> M, f, b, \epsilon, \gamma) = \pi b^2 \hat{\sigma}_n(> M, f, \epsilon, \gamma)$

We assume a selection function that detects all images with flux ratios between the

brightest and faintest images smaller than $f$ with a circular critical radius in the range $\theta_{min} < 2b < \theta_{max}$. For the distribution of galaxies, we assume a Schechter (1976) function exponent of $\alpha = -1$ and a "Faber-Jackson" exponent of $\gamma_{FJ} = 4$ to describe the number counts of galaxies and the relation between luminosity and the velocity dispersion of the isothermal sphere,

$$\frac{dn}{dL} = \frac{n_*}{L_*}\left[\frac{L}{L_*}\right]^{\alpha} \exp(-L/L_*) \qquad \text{and} \qquad \frac{L}{L_*} = \left[\frac{\sigma}{\sigma_*}\right]^{\gamma_{FJ}}, \tag{19}$$

where $n_* = (0.61 \pm 0.21)h^3 10^{-2}$ Mpc$^{-3}$ is the local comoving density of E and S0 galaxies (Loveday et al. 1992, Marzke et al. 1994), and $\sigma_* = (220 \pm 20)$ km s$^{-1}$ is the (dark-matter) velocity dispersion of an $L_*$ galaxy (Kochanek 1993, 1994, Breimer & Sanders 1993, Franx 1993). The optical depth to lensing for SIS lenses in flat cosmologies is $\tau = \tau_*(D_{OS}/r_H)^3/30$ (Turner 1990). The optical depth scale is $\tau_* = 16\pi^3 n_* r_H^3 (\sigma_*/c)^4 \Gamma[1 + \alpha + 4/\gamma_{FJ}] = 0.024 \pm 0.012$, where the uncertainties are dominated by $n_*$ and $\sigma_*$. We perform all calculations in an $\Omega_0 = 1$ cosmological model.

If the probability distribution of the ellipticity parameters is $dP/d\gamma d\epsilon$ and we assume that the orientations of the external shear and the major axis of the galaxy are uncorrelated, then the probability that a source of flux $F$ is lensed to produce $n$ images is

$$P_n(F) = \tau_* D_{OS}^3 \int_0^1 dx x^2(1-x)^2 \int d\epsilon d\gamma \frac{dP}{d\gamma d\epsilon} \hat{\sigma}_n(\gamma,\epsilon) B_n(F,\gamma,r) \left(e^{-u_{min}} - e^{-u_{max}}\right) \tag{20}$$

where $x = D_{OL}/D_{OS}$, $u_{min} = \Delta\theta_{min}^2/\Delta\theta_*^2(1-x)^2$ and $u_{max} = \Delta\theta_{max}^2/\Delta\theta_*^2(1-x)^2$ specify the detectable range of separations where the characteristic image separation is $\Delta\theta_* = 8\pi(\sigma_*/c)^2 = 2\farcs8(\sigma_*/220 \text{ km s}^{-1})^2$ and we assumed that $\alpha = -1$ and $\gamma_{FJ} = 4$. The magnification bias function is

$$B_n(F,\gamma,r) = \left[\frac{dN}{d\ln F}\right]^{-1} \int_0^{\infty} dM \frac{dP_n}{dM}(f,\epsilon,\gamma) \frac{dN}{d\ln F}\left(\frac{F}{M}\right) \tag{21}$$

where $dN/d\ln F$ is the logarithmic number counts distribution of the sources at fixed redshift. The magnification probability distributions $dP_n/dM$ are computed by standard numerical methods (Kochanek & Blandford 1987, Kochanek & Apostolakis 1988, Wallington & Narayan 1993). We use the quasar number counts model detailed in Kochanek (1996a), and the Dunlop & Peacock (1990) pure luminosity evolution number counts model for flat spectrum radio sources (see Kochanek (1996b) for a discussion of uncertainties in the radio luminosity function and its effects on gravitational lensing).

## 4. Elliptical Galaxies

The simplest model for the origin of asymmetries in gravitational lenses assumes that it is due to the ellipticity of the primary lens galaxy. We treat two such models, using either a singular isothermal ellipsoid or a singular isothermal sphere in an external shear field. We first discuss the expected analytic scalings. Next we discuss the ellipticities needed to produce the observed distribution of image morphologies and to fit the individual lenses. We compare the models to the observed lens galaxy where data are available. Finally, we find the best fit parameters of a simple galaxy ellipticity distribution for jointly fitting the number and properties of the observed lenses.

For the isothermal ellipsoid the asymptotic integral cross section for four-image systems is $P(>M) = 4\pi b^2\eta^2/(1-\epsilon^2)^{1/2}M^2$, and to lowest order in $\epsilon$ the total four-image cross section is $\sigma_4 = \pi b^2\eta^2\epsilon^2/6$ (see Kormann et al. 1994b). The minimum magnification of a four-image system, estimated by $P(>M_{min}) = \sigma_4$ is $M_{min} = 24^{1/2}/\epsilon$. For a source at the origin behind the lens, the images form a cross on the major and minor axes of axis ratio $q_c = 1 - \epsilon/3$. To lowest order in the ellipticity $\epsilon = 3(1-q_c)$, so $\sigma_4 = 3\pi(1-q_c)^2b^2\eta^2/2$ and $M_{min} = (8/3)^{1/2}/(1-q_c)$ for model eccentricities chosen to fit the observed ellipticity of a cruciform lens. The external shear model consists of an SIS lens in a quadrupole shear potential (an $F_{OS}$ shear term in eqn. (1)). The asymptotic integral cross-section for four-image systems is $P_4(>M) = 4\pi b^2/M^2$, the total four-image cross section is $\sigma_4 = 3\pi b^2\gamma^2/2$,and the minimum magnification is $M_{min} = 8^{1/2}/\gamma$. For the external shear model to have the same four-image cross section as the ellipsoid model requires $\gamma = \epsilon/3$, and when $\gamma = \epsilon/3$ the four-image magnification probability distributions of the two models are identical to lowest order in $\gamma$ and $\epsilon$. In a symmetric cruciform lens, the axis ratio of the images is $q_c = (1-\gamma)/(1+\gamma)$ so $\gamma = (1-q_c)/2$. For the external shear model to produce the same ellipticity cruciform image requires $\gamma = \epsilon/6$. Fixed to the same axis ratio lens, the external shear model has one-fourth the four-image cross section of the ellipsoid and twice the minimum magnification.

Figure 3 shows the expected number of lenses in the JVAS radio survey and the optical quasar sample for the ellipsoid model and for the external shear model. When we compare models as a function of $\epsilon = 3\gamma$, the results are identical in the low ellipticity limit, and then slowly diverge for large ellipticities. The numbers of four-image lenses exceed the numbers of two-image lenses at moderately high ellipticities. If $\epsilon \gtrsim 0.73$ or $\gamma > 1/3$, two of the cusps extend into the three-image region allowing the production of the three-image cusp geometry. Very flattened ellipsoids are dominated by the cusp image geometry (Kassiola & Kovner 1993) and produce diverging numbers of lenses. The external shear models are eventually dominated by the three-image cusp systems, but not until $\gamma \gtrsim 0.4$ (off the

right edge of Figure 3). Thus, there is a limit to the fraction of lenses that can have the four-image geometry of approximately 60-70%, and the ellipticity must be very finely tuned to reach this limit. Low ellipticity lenses are dominated by the two-image geometry and high ellipticity lenses are dominated by the three-image cusp geometry.

The compact-source part of the JVAS radio sample has equal numbers of two- and four-image lenses, requiring a typical ellipticity parameter of $\epsilon \sim 0.7$ or a typical shear of $\gamma \sim 0.30$. The small number of lenses in the sample (two of each morphology) means that the mean ellipticity is not well determined (see King et al. 1996, Kochanek 1996b). In the quasar sample the greater magnification bias increases the relative numbers of four-image systems compared to the radio sample. The observed ratio of 2 four-image and 3 two-image lenses is produced for $\epsilon \simeq 0.55$ or $\gamma \simeq 0.20$.

For comparison, Table 2 summarizes the best fit models for the lenses found in these surveys using the same two lens models. The ellipsoid and the external shear models have comparable fits to the positions and flux ratios of the lenses, but neither model provides a statistically acceptable fit to any of the four-image lenses. The models have only five parameters, compared to nine or eleven constraints for a four-image lens depending on whether there is an observed lens position, so the parameter values of the best fitting model are well specified even if the absolute goodness of fit is low. Figure 4 shows the probability distributions for the ellipticity parameter ($\epsilon$ or $\gamma$) of the models using the same horizontal scale as in Figure 3. Qualitatively, the ellipticities of the ellipsoidal lens models are approximately equal to the ellipticities needed to produce the observed relative numbers of two- and four-image lenses, while the shears of the external shear models are too low. The two-image lenses are well fit by the models due to the lack of constraints ($N_{dof} = 0$!) and have broad uncertainties in their parameters. As we expect, the eccentricities of the two-image systems are lower than the eccentricities of the four-image systems. The notes to Table 2 summarize the parameters found in other identically parametrized models of these lenses. The results are generally consistent, although most parameter estimates did not include uncertainties and used older, less accurate observational data.

For three lenses, MG 0414+0534, B 1422+231 and 0142–100, we can compare the model ellipticities and orientations to the images of the lens galaxy. The models of MG 0414+0534 (model axis ratio $0.63 \pm 0.02$, optical axis ratio $0.80 \pm 0.02$ (Falco et al. (1996a)) and B 1422+231 (model axis ratio $0.37 \pm 0.01$, optical axis ratio $0.80 \pm 0.02$ (Impey et al. 1996)) are flatter than the optical galaxy, while the model of 0142–100 (model axis ratio $0.80 \pm 0.12$, optical axis ratio $0.71 \pm 0.05$, (Falco et al. 1996b)) is rounder than the optical galaxy. The B 1422+231 model is dramatically flatter than the lens galaxy, and Hogg & Blandford (1994) suggest that shear from two nearby galaxies causes the high axis ratios

Table 2: Elliptical Galaxy Models

| Lens | $N_{dof}$ | Ellipsoid | | | External Shear | | |
|---|---|---|---|---|---|---|---|
| | | $\epsilon$ | $\theta_\epsilon$ | $\chi^2$ | $\gamma_e$ | $\theta_\gamma$ | $\chi^2$ |
| PG 1115+080 | 6 | $0.605 \pm 0.017$ | 66.6° | 150.7 | $0.126 \pm 0.004$ | 65.3° | 82.1 |
| H 1413+117 | 4 | $0.580 \pm 0.014$ | 21.6° | 148.9 | $0.110 \pm 0.003$ | 21.7° | 142.0 |
| MG 0414+0534 | 6 | $0.438 \pm 0.025$ | 79.1° | 110.7 | $0.098 \pm 0.007$ | 78.0° | 116.5 |
| B 1422+231 | 6 | $0.764 \pm 0.006$ | 126.8° | 124.0 | $0.261 \pm 0.004$ | 125.7° | 40.3 |
| 0142–100 | 0 | $0.211 \pm 0.141$ | 105.0° | 0.0 | $0.069 \pm 0.047$ | 106.2° | 0.0 |
| B 0218+357 | 0 | $0.111 \pm 0.072$ | 73.7° | 0.0 | $0.035 \pm 0.024$ | 73.1° | 0.0 |

Notes – The angles $\theta_\epsilon$ and $\theta_\gamma$ are the P.A.s of the major axis of the model. The P.A. uncertainties in the four-image lenses of 0.3° or less are so much smaller than the uncertainties in any P.A. measurement for a lens galaxy (see Table 1) that we do not include them. The errors for the two-image lenses are (+13°, −28°) for 0142–100, and (+40°, −5°) for B 0218+357.

- Related models of PG 1115+080: Kochanek (1991) found $\gamma = 0.08 \pm 0.01$ and $\theta_\gamma = 66° \pm 6°$ based on early ground based data with no lens position.

- Related models of H 1413+117: Kochanek (1991) found $\gamma = 0.11 \pm 0.01$ and $\theta_\gamma = 22° \pm 3°$ based on early ground based data.

- Related models of MG 0414+0534: Kochanek (1991) found $\gamma = 0.08 \pm 0.02$ and $\theta_\gamma = 80° \pm 7°$ based on early ground based data with no lens position. Falco et al. (1996a) found $\gamma = 0.12 \pm 0.03$ and $\theta_\gamma = 77.4° \pm 0.1°$.

- Related models of B 1422+231: Hogg & Blandford (1994) found a model with $\gamma \simeq 0.29$ with $\theta_\gamma \simeq 124°$, and Kormann et al. (1994b) found a model with $\epsilon = 0.71$ and $\theta_\epsilon = 124°$. Our data differs in using the precise position of the lens galaxy from Impey et al. (1996).

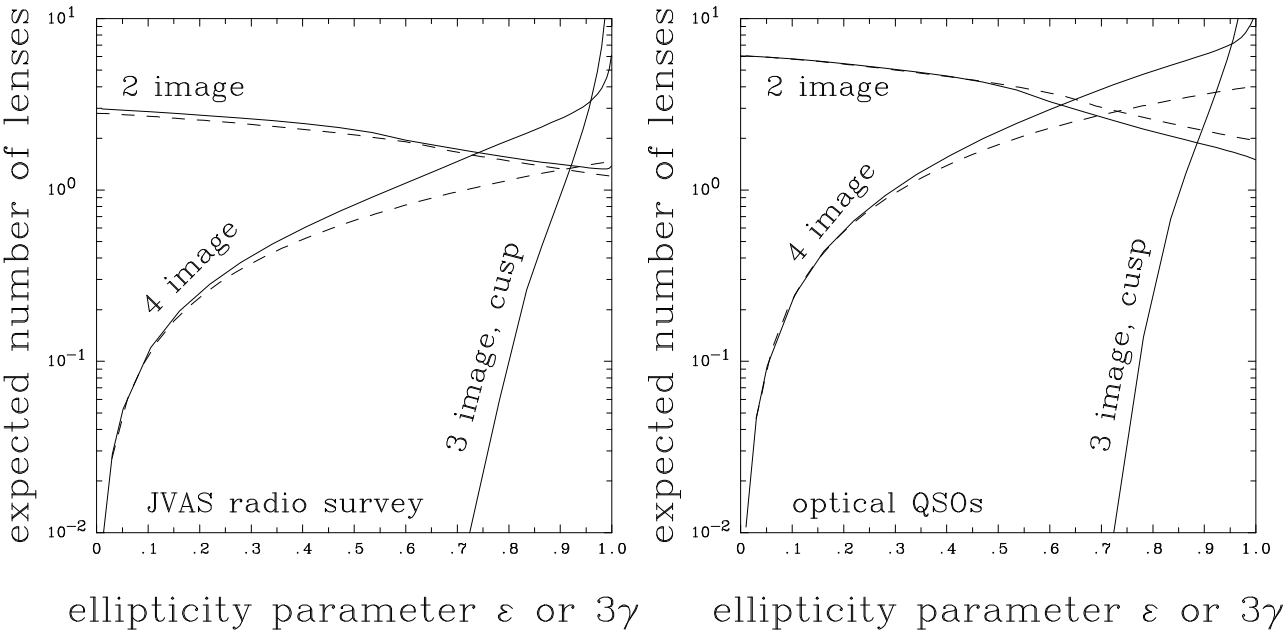


Fig. 3.— The expected number of two-image, four-image, and three-image cusp lenses in the JVAS radio survey (left) and the optical quasar surveys (right) as a function of the ellipsoid parameter $\epsilon$ (solid) or the external shear $\gamma$ (dashed). The horizontal scale is either $\epsilon$ or $3\gamma$ so that in the limit of small ellipticity the models have the same cross-sections and magnification probability distributions. The external shear models have a non-zero three-image cusp cross section for $3\gamma > 1$.

in single shear models of B 1422+231. The perturbing galaxies must be very massive to produce a total shear of $\gamma = 0.26$. Changing the monopole of the lens to be more centrally concentrated and closer to a constant mass-to-light ratio model will generally increase the model ellipticities and exacerbate the differences (see Kochanek 1991a, Wambsganss & Paczyński 1994, Keeton & Kochanek 1996b). If the angular structure of the lens is entirely due to an ellipsoid aligned with the luminous galaxy, then the lens model should be aligned with the visible image of the galaxy independent of the radial profile of the monopole. Misalignments between the models and the lens galaxy must be due either to external shears or misalignment of the galaxy and its dark matter halo. The position angles of the major axes of the light distribution and the model differ by $8^\circ \pm 5^\circ$ for MG 0414+0534 and by $6^\circ \pm 15^\circ$ in B 1422+231. The misalignment in MG 0414+0534 is significant, although smaller than the $30^\circ \pm 15^\circ$ misalignment observed in the X-ray halo of NGC 720 (Buote & Canizares 1994, 1996). For the two-image lens 0142–100 the misalignment is $32^\circ\,^{+18}_{-33}$, where the uncertainty is dominated by the underconstrained lens model.

We next assume an ellipticity distribution for the lens galaxies and look for the maximum likelihood distribution that simultaneously agrees with the model ellipticities and the observed numbers of lenses. To simplify the comparison of the ellipsoid and external shear models to the data, we assumed the same Gaussian distribution for $\epsilon$ used in §2.1 to fit the observed axis ratios of galaxies. Figure 5 shows likelihood contours for the two parameters of fitting both the relative numbers of two- and four-image systems as well as the observed parameters of the lenses. The best fit ellipsoid distribution is $\epsilon_0 = 0.38$ and $\Delta\epsilon_0 = 0.22$, although there is a broad class of acceptable solutions running to lower $\epsilon_0$ and larger distribution widths. The best fit parameter values for the Coma galaxies from §2.1 ($\epsilon_0 = 0.26$, $\Delta\epsilon = 0.33$) lie well within the 90% confidence likelihood contour at 77% of the peak likelihood. Figure 5 also shows the eccentricity distribution of the Coma galaxies, and the two best fit Gaussians. The best fit to the lens data has fewer of both high and low eccentricity galaxies than the fit to the observed axis ratios. Our use of $\eta = 1$ in normalizing the lens model (see §2.1) may mean we are overestimating the number of high ellipticity galaxies needed to fit the lens data. The best fit external shear distribution has $\gamma_0 = 0.076$ and $\Delta\gamma_0 = 0.089$, again with a flat likelihood function towards lower shear and greater widths. The best fit ellipsoid model has a significantly higher likelihood than the best fit external shear model, with a likelihood ratio of 36% between the two best fitting models. The lower relative likelihood of the external shear models is due to the mismatch between the shear required to produce the observed numbers of four-image lenses and the shear required to fit the lenses.

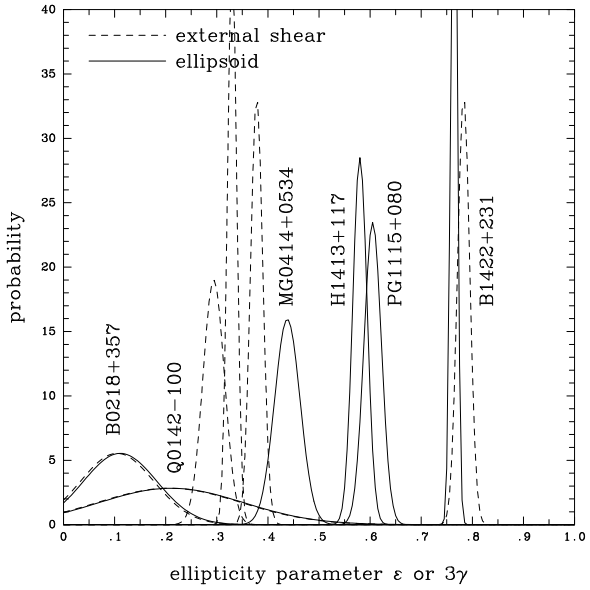


Fig. 4.— Ellipticity $\epsilon$ (solid) or external shear $\gamma$ (dashed) probability distributions for the modeled lenses. The horizontal scale is either $\epsilon$ or $3\gamma$ so that in the limit of small ellipticity the models have the same cross-sections and magnification probability distributions. The ordering of the lenses in shear and ellipticity is the same.

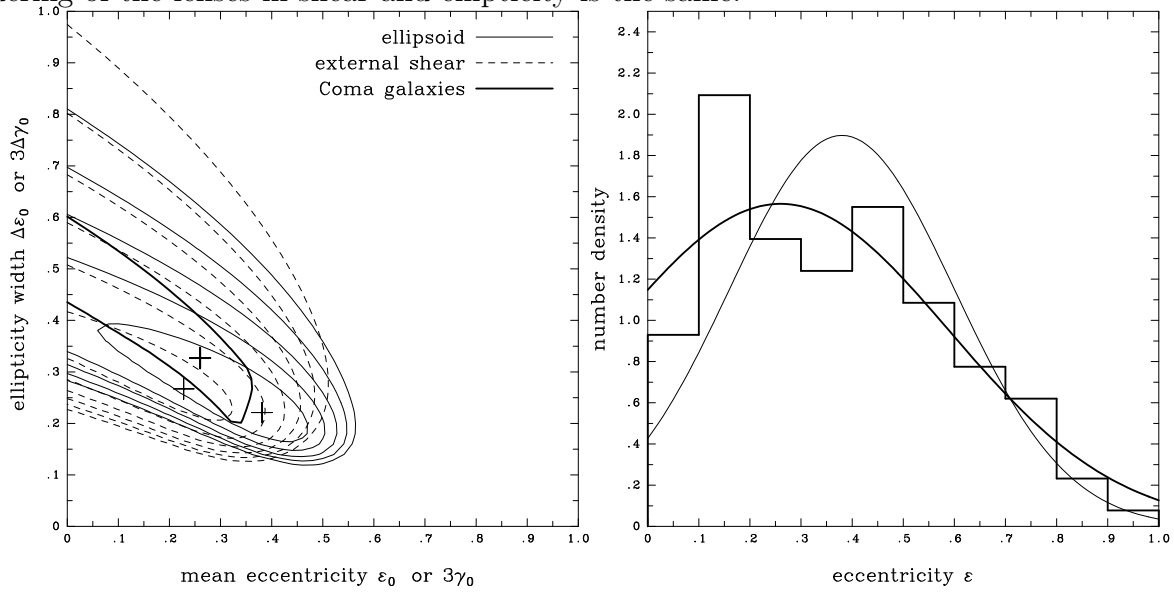


Fig. 5.— Best fit Gaussian eccentricity (solid), external shear (dashed) or Coma galaxy (heavy solid) distributions. The left panel shows likelihood contours for the fits. The crosses mark the peak likelihood models and the contours are spaced at 0.1 dex from the maximum. The lowest contour is the maximum likelihood 90% confidence region for two parameters. The peak likelihood of the external shear model is only 36% that of the ellipsoid model. The heavy solid contour shows the 90% confidence contour for the fits to the E+S0 galaxy sample in Coma. The right panel shows a histogram of the Coma sample, the best fit Gaussian eccentricity distribution to the Coma sample (heavy solid), and the best fit distribution to the lens data for the singular isothermal ellipsoid model (light solid).

## 5. Multiple Shear Models

The ellipsoidal models of §4 reproduce the observational data in a statistical sense. A population of singular isothermal ellipsoids with the axis ratio distribution of the early type galaxies in Coma is compatible with the lens data, although the best fitting models are slightly more elliptical. In our small sample, there is no evidence for large misalignments between the models and the observed galaxies, although the model and observed axis ratios differ. The ellipsoidal models are more consistent with the data than the external shear models. There are, however, two problems. The first problem is B 1422+231, where the axis ratio of the lens model ($0.37 \pm 0.01$) is flatter than both the observed galaxy ($0.80 \pm 0.02$) and the typical Coma E/S0 galaxy (6% of the Jørgensen & Franx (1994) galaxies, all S0s, are flatter than the model). The second problem is that none of the four-image lenses is well fit by either single shear model, and we know from Kochanek (1991a), Wambsganss & Paczyński (1994), and Keeton & Kochanek (1996b) that changing the monopole structure of the lens generally does not lead to an acceptable fit. From the analyses in §2, we expect all lenses to have an external shear perturbation in addition to the primary lens. Here we consider lens models with two sources of shear, consisting either of an ellipsoidal galaxy in an external shear field, or a LSS shear model ($F_e$ and $F_{OL}$), and determine how the additional shear influences the statistics and model fitting.

We first estimate the numbers of lenses of different morphologies. Figure 6 shows the expected numbers of lenses as a function of $\gamma$ and $\epsilon$ averaged over their relative orientations and assuming that the shear is constant with source and lens redshift. The average optical depth for four-image lenses varies with the sum in quadrature of the ellipticity and the shear, $\tau_4 \propto \epsilon^2 + (3\gamma)^2$, unless the primary lens is very flattened. In the Coma galaxy sample (Jørgensen & Franx 1994) the rms eccentricity is $\langle \epsilon^2 \rangle^{1/2} \simeq 0.43$, so the typical shear must be of order $\gamma \sim 0.15$ before it is an important perturbation to lens statistics. Moreover, all the perturbative shear sources discussed in §2 depend strongly on the source and lens redshifts so the typical shears are considerably lower than the peak shears. Figure 7 shows the expected number of four image lenses as a function of primary lens eccentricity and the maximum rms LSS shear $\gamma_m$ (see §2.3) for a source at $D_{OS}/r_H = 1$ ($z_s \simeq 3$). We assumed that the two components of the effective shear were Gaussian random variables for fixed lens and source redshift with an rms effective shear of $\gamma_e^2 = 16\gamma_m^2 x^2 (1-x)^2 (D_{OS}/r_H)^3$. The LSS shear does not significantly increase the production of four-image lenses unless the primary lens is nearly circular ($q_2 \gtrsim 0.9$). The ratio of the four-image to the total optical depth in the Gaussian LSS shear model is $N_4/N_T \simeq \gamma_m^2 (D_{OS}/r_H)^3/14 + \langle \epsilon^2 \rangle/6$, so $\gamma_m \simeq 0.65 (D_{OS}/r_H)^{-3/2}$ is needed to make the external shear as important as the intrinsic ellipticity. Unless the estimates in §2 for the external shear ($\gamma_m \simeq 0.05 (D_{OS}/r_H)^{-3/2}$) are wrong by an order of magnitude, the lens cross sections and probabilities are dominated

Table 3: Two Shear Models

| | | Ellipsoid + External Shear | | | | SIS + LSS Shear | | | |
|---|---|---|---|---|---|---|---|---|---|
| Lens | $N_{dof}$ | $\chi^2_{min}$ | $\epsilon$ | $\gamma$ | $\lvert\Delta\theta\rvert$ | $\chi^2_{min}$ | $\gamma_e$ | $\gamma_{OL}$ | $\lvert\Delta\theta\rvert$ |
| PG 1115+080 | 4 | 2.0 | 0.22 | 0.09 | 36° | 2.2 | 0.12 | 0.04 | 40° |
| H 1413+117 | 2 | 0.1 | 0.40 | 0.19 | 80° | 0.5 | 0.13 | 0.12 | 89° |
| MG 0414+0534 | 4 | 12.1 | 0.38 | 0.17 | 86° | 48.9 | 0.09 | 0.06 | 58° |
| B 1422+231 | 4 | 33.7 | 0.22 | 0.20 | 3° | 33.3 | 0.23 | 0.05 | 4° |

- Related Models of B 1422+231: Kormann et al. (1994b) found models with parameters $\epsilon = 0.47$, $\gamma = 0.16$ and $|\delta\theta| = 4°$ (model 3a) and $\epsilon = 0.51$, $\gamma = 0.10$ and $|\delta\theta| = 11°$ (model 3b). Model 3a lies along the continuation of the $\chi^2$ ridge towards higher ellipticities, while model 3b is well below the ridge. Our data differs in using the precise position of the lens galaxy from Impey et al. (1996).

by the intrinsic properties of the primary lens galaxy. Similar calculations show that the other sources of external shear perturbations discussed in §2.2-2.4 are also too weak to significantly change the expected numbers of lenses of different morphologies.

When we model the lenses with two shear terms we are adding two extra parameters to the models and expect a reduction in the resulting $\chi^2$. We consider two models, a singular isothermal ellipsoid in an external shear (in eqn. (1) with $F_{LS} = F_{OL} = 0$), and a SIS with LSS shear (in eqn. (1) with $F_{LS} = 0$, and $\epsilon = 0$). Kochanek (1991a), Wambsganss & Paczyński (1994), and Keeton & Kochanek (1996b) find that adding two extra parameters to the radial (monopole) structure of the lens model usually does not dramatically improve the goodness of fit over the simple SIS + external shear model. Only when the lens has extended radial structure, as in the radio rings (see Kochanek 1995), do we expect the models to depend strongly on the radial structure (Kochanek 1991a). When we add two parameters to the model in the form of an additional shear term, however, the $\chi^2$ of the model fits to our lens sample improve dramatically (see Table 3). The $\chi^2$ of the PG 1115+080 and H 1413+117 models are statistically acceptable, the $\chi^2$ of the ellipsoid + external shear model of MG 0414+0534 is marginally acceptable, and the $\chi^2$ of the B 1422+231 models and the LSS model of MG 0414+0534 are at least greatly improved. The two image lenses (0142–100 and B 0218+357) models are underconstrained (negative degrees of freedom) and were not included. *Independent of the origins of the extra shear, it is a more fundamental variable in models of point-image lenses than variations in the monopole structure.* We expect lens models to be more sensitive to multiple shear axes than statistics for two reasons. First, the corrections to the lens model from the extra shear

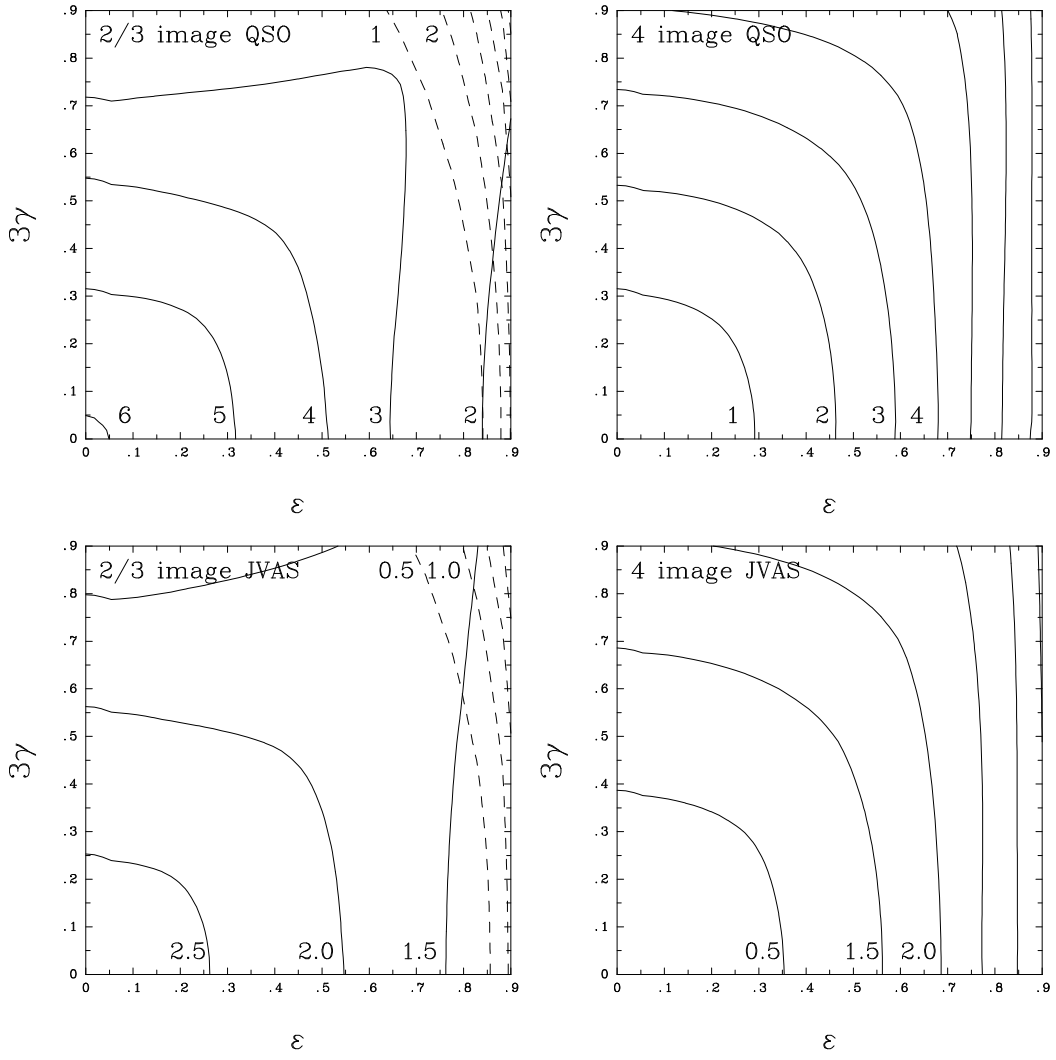


Fig. 6.— Expected numbers of lenses in the quasar (top) and JVAS (bottom) lens samples as a function of the axis ratio of the isothermal ellipsoid $r$ and the external shear field $\gamma$. In the 2/3 image figures, the numbers of two image systems are shown by the solid contours, and the number of three image systems by the dashed contours. The numbers label the nearest contour.

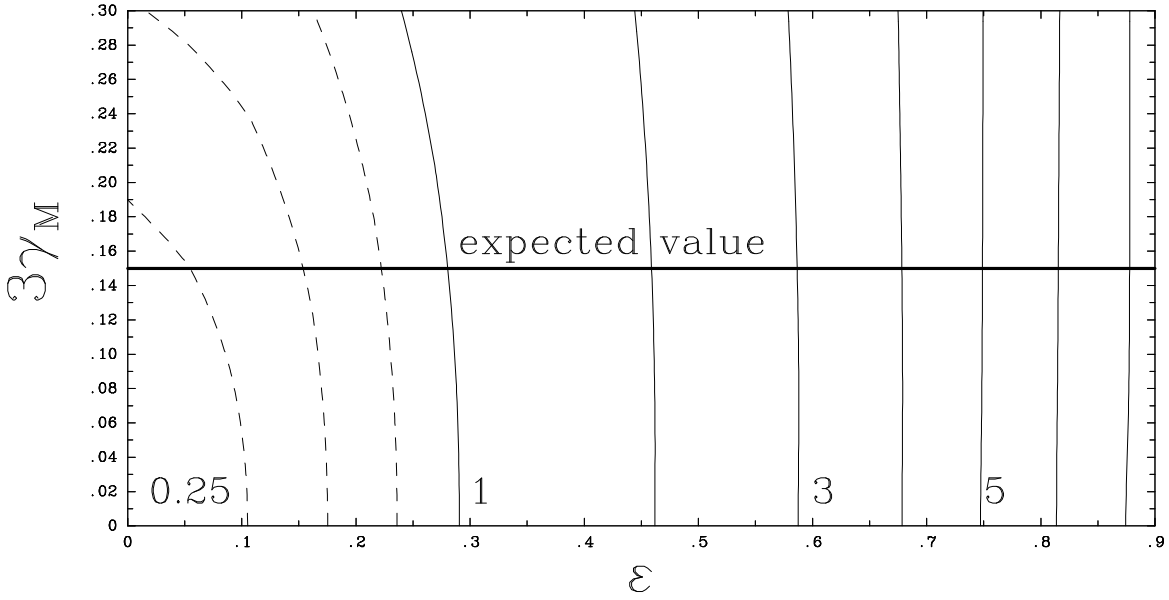


Fig. 7.— Expected number of four-image quasar lenses as a function of the maximum rms LSS shear at $D_{OS}/r_H = 1$, $\gamma_m$. The horizontal line marks the expected value from §2.3. The solid contours are spaced in steps of one lens, and the dashed contours in steps of 0.25 lenses. The numbers label the nearest contour.

are (to lowest order) linear in the shear rather than quadratic. Second, models with two shear axes are qualitatively different from single shear models, so no single shear model can generically mimic the lensing properties of a two shear model. Although two shear axes introduce some qualitative changes in the statistical properties (e.g. allowing a 6 image lens), they are related to rare and (so far) unobserved events. We also fit the lenses with the external shear forced to be parallel or perpendicular to the ellipsoid to test whether the improvement in the fits could be caused by changes in the balance between the internal and external quadrupole moments rather than misalignment. The minimum $\chi^2$s for these models were 83.4, 142.5, 108.1, and 35.2 for PG 1115+080, H 1413+117, MG 0414+0534 and B 1422+231 respectively. Except for B 1422+231, where the shears must be aligned to within a few degrees even in the unconstrained models, the $\chi^2$ are much closer to the $\chi^2$ of the single ellipticity models of Table 2 than the unconstrained models in Table 3.

Most of the two shear models do not lead to unique solutions, so we list only the model parameters at the minimum of the $\chi^2$ in Table 3. Figure 8 shows contours of the $\chi^2$ in the space of $\epsilon$ and $\gamma$ after optimizing all other parameters. The $\chi^2$ contours in the $\epsilon$–$\gamma$ plane generically have the "U" shape seen in the PG 1115+080 and H 1413+117 contours. One side of the U, the "additive branch," has $\epsilon + 3\gamma$ nearly constant. Along the additive branch the angle between the major axes of the shear and the ellipsoid is slowly varying and has no specific value ($\sim 30^\circ$ in PG 1115+080, $\sim 40^\circ$ in H 1413+117, and $\sim 2^\circ$ in B 1422+231). Along the other two sides of the U, the "cancellation branches," the shear and the ellipticity increase in magnitude but become perpendicular. The $\chi^2$ varies along the $U$, and different lenses have minima at different points. H 1413+117 has its minimum $\chi^2$ on one of the cancellation branches with a tail extending toward the additive branch. MG 0414+0534 has acceptable solutions only on one of the cancellation branches, and B 1422+231 has acceptable solutions only on the additive branch. The $\chi^2$ contours of the LSS models (not shown) are qualitatively different, with the value of $\gamma_e$ nearly fixed as $\gamma_{OL}$ varies. If we add the observed major axis of the lens as a constraint for the models of MG0414+0534, then the best fit model has $\chi^2 = 66.1$ for $N_{dof} = 5$, significantly worse than for models in which the angle was free to vary. In the unconstrained solution the PA of the major axis is $2^\circ$, compared to the measured PA of $71^\circ \pm 5^\circ$. With the constraint, the best solution shifts to the other cancellation branch, with a galaxy PA of $75^\circ$, axis ratio of 0.44 ($\epsilon = 0.68$), and an external shear of $\gamma = 0.10$. On this branch of the solutions, the galaxy PA is almost exactly fit, at the price of significantly worse fits to the positions and flux ratios.

Figure 8 also shows the integral probability distributions for either the LSS effective shear (assuming Gaussian statistics) or the correlated shear for each of the four lenses. The magnitudes of the shear perturbations required to fit the lenses are significantly larger than the expected external shears in all cases. We know from the statistical models that the

probability of finding a four-image lens is not significantly enhanced by the external shear sources discussed in §2 unless the primary lens is nearly circular or the estimates of the shear are gross underestimates. While we could explain the high values of the secondary shears in one of these lenses using external shear perturbations (the best candidate being B 1422+231, Hogg & Blandford 1994), it is extraordinarily unlikely that all could be explained by external shear perturbations. *Unless §2.2–§2.4 grossly underestimate the typical external shear perturbations, the secondary shear must also be dominated by the primary lens galaxy rather than external perturbations.* We defer a discussion of the implications to the conclusions.

If we use a single-shear model for a lens with two independent shear axes, one of which is aligned with the luminous galaxy, then the major axis of the model will not be aligned with the luminous galaxy. To estimate misalignment angles we used the position angle of the cruciform quad lens formed by placing the source directly behind the ellipsoid + external shear lens model. The misalignment angle of the images $\Delta\theta_I$ relative to the ellipsoid computed to first order in the eccentricity is

$$\tan 2\Delta\theta_I = \frac{3\gamma \sin 2\Delta\theta}{\epsilon + 3\gamma \cos 2\Delta\theta} \tag{22}$$

where $\Delta\theta$ is the angle between the ellipsoid and the external shear. Figure 9 shows the mean misalignment angle and its standard deviation for the average lensed quasar including all variations in cross section and magnification bias with the angle between the shear and the ellipsoid for primary lens galaxies with axis ratios of $q_2 = 0.9$, 0.7, and 0.5. For $\gamma \gg \epsilon$, the distribution is uniform in the misalignment angle with a mean of $\langle \Delta\theta_I \rangle = 45^\circ \pm 26^\circ$. For $\gamma \ll \epsilon$ the lens probability is independent of $\gamma$ and the mean misalignment approaches $(55^\circ \pm 26^\circ)\gamma/\epsilon$ ($5.5^\circ$ for $\gamma = 0.01$ and $\epsilon = 0.1$). The four-image lensing probability is enhanced if the shear is aligned with the ellipsoid, while the two-image lensing probability is enhanced if the shear is perpendicular, so two-image systems will show larger average misalignments than four-image systems for a fixed axis ratio and shear. Unless the lens galaxy is very circular or the shear is larger than 10%, four image systems should rarely show misalignments exceeding $\sim 20^\circ$. Interestingly, the model of the two-image lens 0142–100 shows the largest misalignment, although the large uncertainties make the models technically consistent with no misalignment.

## 6. Conclusions

The most important source of ellipticity in gravitational lenses is the primary lens galaxy. Early-type E and S0 galaxies produce most gravitational lenses, and the observed

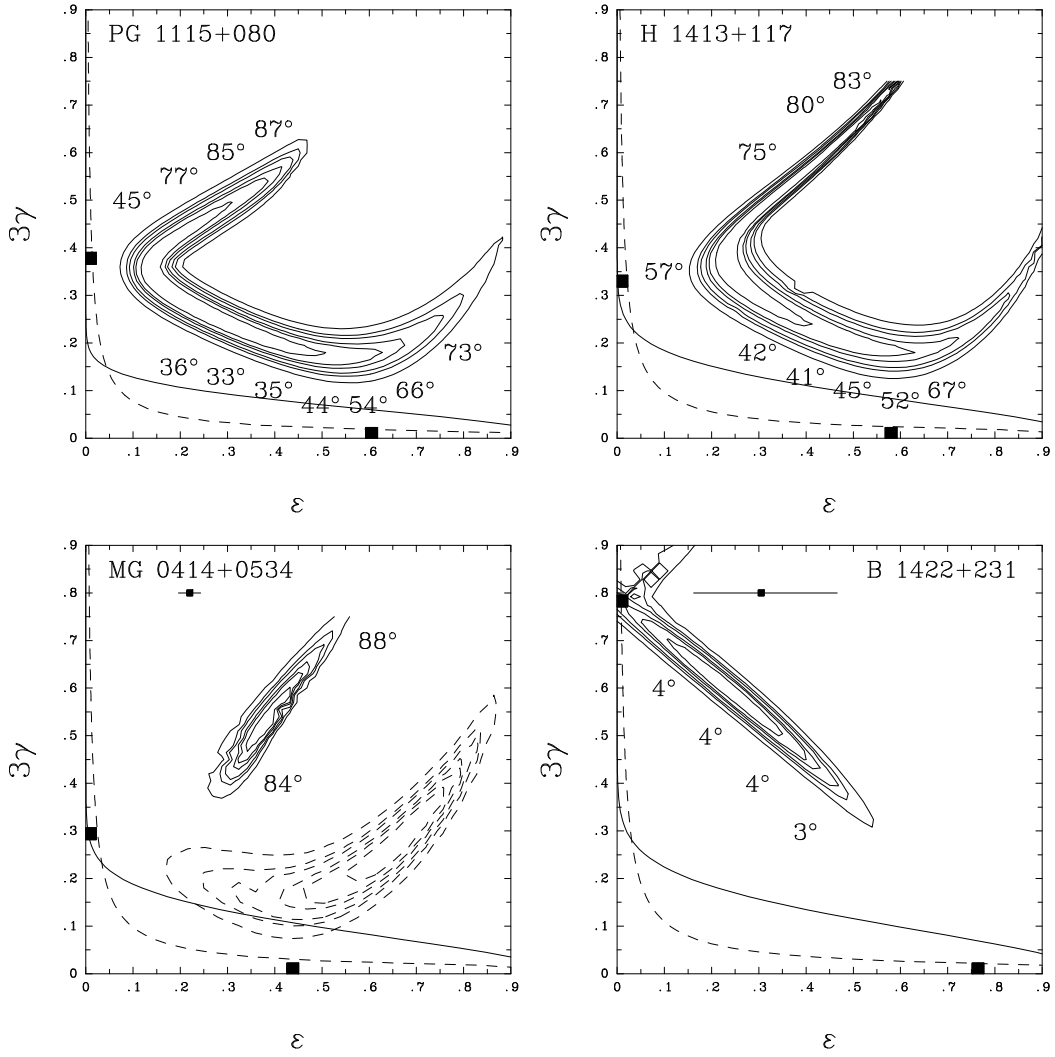


Fig. 8.— Contours of $\Delta\chi^2$ in the plane of $\epsilon$ and $\gamma$ for the four-image lenses. Contours are drawn at $\Delta\chi^2 = 2.30$, 4.61, 6.17, 9.21, 11.8, and 18.4, the 1–$\sigma$, 90%, 2–$\sigma$, 99%, 3–$\sigma$, and 99.99% confidence levels for two parameters. The models of PG 1115+080, MG 0414+0534, and B 1422+231 have $N_{dof} = 4$, while the model for H 1413+117 has $N_{dof} = 2$ because the lens position remains unknown. The numbers give the absolute value of the angle between the major axis of the ellipsoid and the shear along the minimum of the $\chi^2$ function. The heavy solid points on the axes mark the solutions from §4, and the points with error bars in the MG 0414+0534 and B 1422+231 panels show the measured eccentricities. The dashed contours in the MG 0414+0534 panel show the $\Delta\chi^2$ contours for models with the PA of the ellipsoid constrained to fit the observations. The two curves on the lower, left side of each panel are the integral probability of a shear exceeding $\gamma$ for the Gaussian LSS shear model (solid) and correlated power-law shear model (dashed) given the redshifts of the lens. The horizontal ($\epsilon$) axis becomes the integral probability. The models assume a rms LSS shear of $\langle\gamma_e^2\rangle^{1/2} = 0.20x(1-x)(D_{OS}/r_H)^{3/2}$ or the correlated shear model of equation (9).

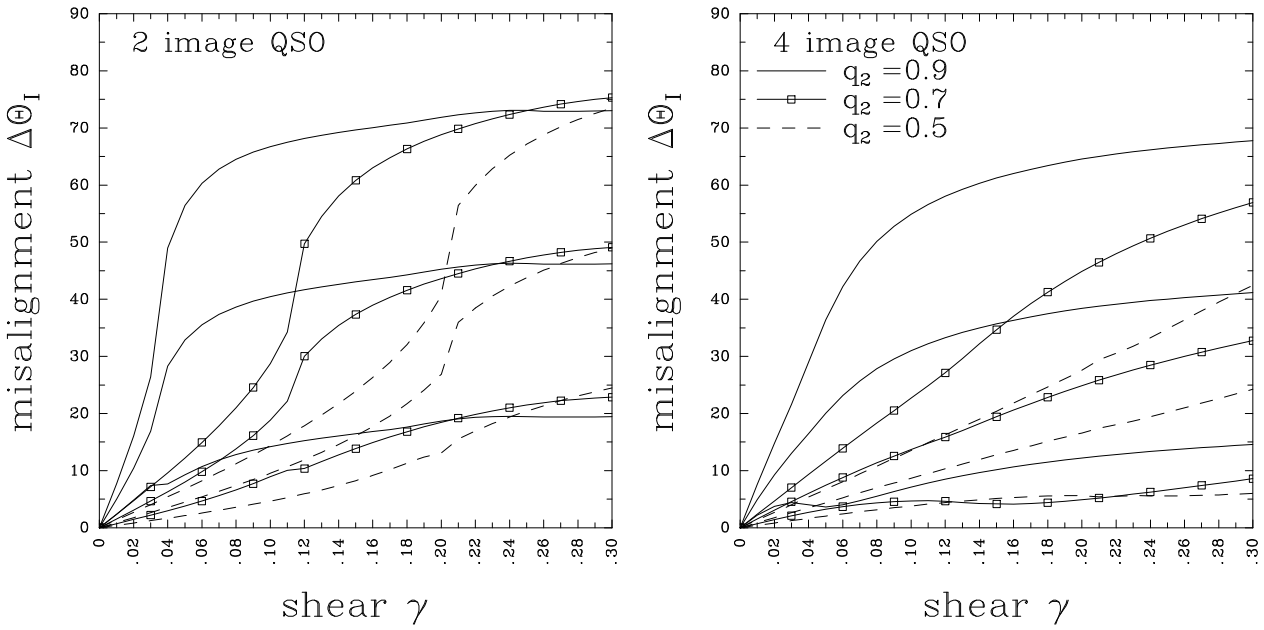


Fig. 9.— Mean misalignment angle for two-image (left) and four-image (right) quasar lenses. The solid lines, solid lines with points, and dashed lines are for primary lenses with axis ratios of $q_2 = 0.9$, 0.7, and 0.5 respectively. There are three lines for each axis ratio. The central line is the mean, and the upper (lower) line is the mean plus (minus) one standard deviation. A uniform random distribution in the misalignment angle has a mean of $45° \pm 26°$, and the uniform limit is reached for the high shear models. External shear perturbations are expected to be smaller than 5% for most lenses.

distribution of projected axis ratios is statistically consistent with the distribution required to produce the observed numbers of gravitational lenses and their ellipticities. We assumed the presence of dark matter by using singular isothermal ellipsoids for the mass distribution, because constant mass-to-light ratio models are known to be inconsistent with the properties of gravitational lenses (Maoz & Rix 1993, Kochanek 1995, 1996a). On average, the models that simultaneously produce the observed numbers of two-image and four-image lenses and are consistent with the ellipticities needed to model the individual lenses are somewhat more elliptical than the light distributions of a sample of E and S0 galaxies in the Coma cluster (Jørgensen & Franx 1994). The best fit lens models have fewer galaxies with axis ratios above 0.75 and below 0.4 than the best fit Coma model, and the normalization of our models may overestimate the required number of high ellipticity galaxies. The ellipticity of a lens model is a function of the monopole structure (Kochanek 1991), and more centrally concentrated, constant mass-to-light ratio models would require higher ellipticities to fit the same data.

In the three cases where we can compare the axis ratio of the model to the axis ratio of the lens galaxy, one model is rounder (0142–100), one model is somewhat flatter (MG 0414+0534), and one model is dramatically flatter (B 1422+231, as noted earlier by Hogg & Blandford (1994) and Kormann et al. (1994b)). In B 1422+231 (Patnaik et al. 1992) the axis ratio of our model is $0.37 \pm 0.01$ while the axis ratio of the galaxy is $0.80 \pm 0.02$ (Impey et al. 1996), even though the major axes of the model and the galaxy are aligned to $6^\circ \pm 15^\circ$. A similar discrepancy is seen in HST 14176+5226 (Ratnatunga et al. 1995, model axis ratio 0.40, galaxy axis ratio 0.68). The major axes of the 0142–100 and B 1422+231 models are aligned with the observed lenses to within the model and photometric uncertainties, while the model is misaligned relative to the galaxy in MG 0414+0535 by $8^\circ \pm 5^\circ$.

Our simple single shear lens models do not fit the four-image lenses very well, with typical $\chi^2/N_{dof} \simeq 20$ for both the singular isothermal ellipsoid and SIS plus external shear models. Studies by Kochanek (1991a), Wambsganss & Paczyński (1994), and Keeton & Kochanek (1996b) show that changing the radial mass distribution of the lens causes little improvement in the fits. Adding an additional external shear that is either aligned or perpendicular to the ellipsoid is of little help in improving the fits. However, when we add an independent external shear that is not forced to be aligned with the ellipsoid, we suddenly find acceptable fits to most of the lenses, with $\chi^2/N_{dof} \lesssim 3$. *Whatever its origin, an independent source of shear appears to be a more fundamental variable than changes in the radial mass distribution.* An independent shear can be produced either by misalignments between the luminous galaxy and the dark matter halo, or by external shear perturbations.

What do we expect for early-type galaxies with dark matter? Numerical simulations

generically find dark matter halos that are both more elliptical and more triaxial than luminous galaxies (e.g. Warren et al. 1992, Dubinski 1992, 1994). Because gravitational lensing depends on the projected mass density of the galaxy, it is far more sensitive to the properties of the halo than most other probes of the angular structure of galaxies. The differences in how the mass distribution is weighted probably explain why dynamical models of ellipticals find a mass to light ratio of $(10 \pm 2)h$ (e.g. van der Marel 1991), while lens models require $(22 \pm 5)h$ (Kochanek 1995, 1996). The triaxiality of galaxies and halos can have two important, qualitative effects on lens models. First, if the halos are more triaxial than the light, as expected from simulations, then the projected ellipticity distribution of the halos will show a larger deficit of low ellipticity systems than is observed in the luminous galaxies. In fact, the most significant difference between the estimated ellipticity distributions for the Jørgensen & Franx (1994) galaxies and the lens models is that the best fit lens models have smaller numbers of low ellipticity galaxies. The lens data requires an ellipticity distribution with fewer round galaxies to produce the observed number of four-image lenses. Secondly, if the triaxialities of the luminous and the halo matter differ, then the projected halo mass distribution and the projected luminosity distribution can be misaligned, producing two different shear axes. In the Franx et al. (1991) study of kinematic misalignments between the major axes the projected rotation axes of elliptical galaxies, 26% of galaxies show misalignments exceeding 30°. Comparable misalignments can appear between the two projected mass distributions, particularly for the lower ellipticity lens galaxies. Differing triaxialities for the luminous matter and the dark matter should also appear as misalignments between optical and X-ray isophotes, such as the $30° \pm 15°$ misalignment seen in NGC 720 (Buote & Canizares 1994, 1996).

The angular structure of the primary lens is not, however, the only source of asymmetries contributing to gravitational lensing. Objects correlated with the primary lens galaxy or near the line of sight add additional external shear perturbations. We estimate that the most important sources of external perturbations are galaxies within a correlation length of the primary lens. The shear contribution from clusters is comparable only if every galaxy is in a cluster. The lowest mass groups and clusters contribute most of the lensing cross section both for multiple imaging (see Kochanek (1995b), Wambsganss et al. (1995)) and external shear perturbations. In the the observed lens sample, the only convincing lens associated with a cluster, 0957+561 (Young et al. 1980), is in a small, diffuse cluster. The PG 1115+080 lens galaxy appears to be part of a small group of galaxies (Young et al. 1981), and the external shear perturbation required to produce a good lens model is consistent with shear from the group (Schechter et al. 1996). The next most important source of external perturbations are other galaxies and clusters along the line of sight (Kochanek & Apostolakis 1988, Jaroszyński 1991). Large external shear perturbations are

associated with discreet objects, usually galaxies, and the perturbing galaxies must be close to the primary lens and will usually have similar or brighter fluxes. The universe is optically thick to shear perturbations of a few percent produced by large scale structure (Kaiser 1992, Seljak 1994, Bar-Kana 1996), and the rms shear fluctuations predicted using non-linear power spectra (Bar-Kana 1996) are quantitatively similar to the shear predicted by adding up the effects of discrete non-linear objects. The probability distribution of the high shear perturbations is a power law, and not the Gaussian distribution assumed in the LSS models. For a source at a redshift of $z_s = 3$, the typical (rms) shear is approximately 3%, and about 5% of lenses will have shear perturbations exceeding 10%.

Such small external shear perturbations have negligible effects on the statistics of gravitational lenses, because ellipsoidal mass distributions are more efficient than external shears in producing four-image gravitational lenses. The typical shear perturbation would have to be an order of magnitude larger than predicted to significantly modify the cross sections and lensing probabilities, and such large shears would be trivially detected in ellipticity correlation function experiments (Mould et al. 1994, Fahlman et al. 1994). Nonetheless, external shear perturbations can be important for models of individual lenses. In particular, lenses such as B 1422+231 that require bizarrely flattened galaxies to fit the data, probably must have strong external shear perturbations. Blandford & Hogg (1994) have shown that there are bright galaxies near B 1422+231 that can produce the necessary shear. Even so, B 1422+231 is a joint effort between the primary lens galaxy and the external shear, because the major axis of the galaxy also has the orientation needed to fit data (Impey et al. 1996). However, since all of our two-shear models required shear perturbations larger than expected for external perturbations, we believe that misalignments due to dark matter halos must be the primary origin of the secondary shear.

Acknowledgements: The authors would like to thank R. Bar-Kana, E. Falco, J. Lehar, E. Ostriker, and P. Schechter for discussions about ellipticity in gravitational lenses and for reading parts of the manuscript. E. Falco kindly supplied data on several of the lenses in advance of publication. C.S.K. is supported by NSF grant AST-9401722.

## REFERENCES

Arnaboldi, M., & Sparke, L.S., 1994, AJ, 107, 958

Bardeen, J.M., Bond, J.R., Kaiser, N., & Szalay, A.S., 1986, ApJ, 304, 15

Bar-Kana, R. 1996, ApJ, 468, 17

Binney, J.J. 1985, MNRAS, 212, 767

Binney, J.J., & Tremaine, S.D. 1987, Galactic Dynamics (Princeton: Princeton University Press)

Breimer, T.G., & Sanders, R.H., 1993, A&A, 274, 96

Blandford, R.D., Saust, A.B., Brainerd, T.G., & Villumsen, J.V. 1991, MNRAS, 251, 600

Brainerd, T.G., Blandford, R.D., & Smail, I., 1996, in Astrophysical Applications of Gravitational Lensing, IAU 173, eds. C.S. Kochanek, & J. N. Hewitt (Dordrecht: Kluwer) 183

de Bruijne, J.H.J., van der Marel, R.P., & de Zeeuw, P.T. 1996, *MNRAS, in press.*

Buote, D.A., & Canizares, C.R. 1994, ApJ, 427, 86

Buote, D.A., & Canizares, C.R. 1996, ApJ, 457, 177

Buote, D.A., & Canizares, C.R. 1996, ApJ, 468, 184

Burke, B.F., Lehàr, J., & Conner, S.R., 1992, Gravitational Lenses, eds. R. Kayser, T. Schramm, & L. Nieser (Springer: Berlin) 237

Carollo, C.M., de Zeeuw, P.T., van der Marel, R.P., Danziger, I.J., & Qian, E.E., 1995, ApJ, 441, L25

Crampton, D., McClure, R.D., & Fletcher, J.M., 1992, ApJ, 392, 23

Dubinski, J. 1992, ApJ, 401, 441

Dubinski, J. 1994, ApJ, 431, 617

Dunlop, J.S., & Peacock, J.A., 1990, MNRAS, 247, 19

Eke, V.R., Cole, S., & Frenk, C., 1996, *preprint*

Fabbiano, G., 1995, in Fresh Views of Elliptical Galaxies, eds., A. Buzzoni, A. Renzini, & A. Serrano, (San Fransisco: ASP) 103

Fahlman, G.G., Kaiser, N., Squires, G., & Woods, D., 1994, ApJ, 437, 56

Falco, E.E., Lehár, J., & Shapiro, I.I., 1996a, *preprint*

Falco, E.E., 1996b, private communication

Franx, M., Illingworth, G., & De Zeeuw, T., 1991, ApJ, 383, 112

Franx, M., 1993, in Galactic Bulges, ed. H. Dejonghe & H.J. Habing (Dordrecht: Kluwer) 243

Fukugita, M., & Turner, E.L. 1991, MNRAS, 253, 99

Grogin, N., & Narayan, R., 1996, ApJ, 464, 92

Gunn, J.E. 1967, ApJ, 147, 61

Henry, J.P., & Arnaud, K.A. 1991, ApJ, 372, 410

Hogg, D.W., & Blandford, R.D., 1994, MNRAS, 268, 889

Impey, C.D., Foltz, C.B., Petry, C.E., Browne, I.W.A., & Patnaik, A.R., 1996, ApJ, 462, 53

Jackson, N., de Bruyn, A.G., Myers, S., Bremer, M.N., Miley, G.K., Schilizzi, R.T., Browne, I.W.A., Nair, S., Wilkinson, P.N., Blandford, R.D., Pearson, T.J., & Readhead, A.C.S., 1995, MNRAS, 274, L25

Jain, B., Mo, H.J., & White, S.D.M. 1995, MNRAS, 276, L25

Jørgensen, I., & Franx, M., 1994, ApJ, 433, 553

Jaroszyński, M. 1991, MNRAS, 249, 430

Jaroszyński, M., Park, C., Paczynski, B., & Gott, J.R., 1990, ApJ, 365, 22

Keeton, C.R., & Kochanek, C.S., 1996b, in preparation

Keeton, C.R., & Kochanek, C.S., 1996a, in in Astrophysical Applications of Gravitational Lensing, IAU 173, eds. C.S. Kochanek, & J. N. Hewitt (Dordrecht: Kluwer) 419

Kaiser, N. 1992, ApJ, 388, 272

Kassiola, A., & Kovner, I. 1993, ApJ, 417, 450

King, L.J., Browne, I. W A., Wilkinson, P.N., & Patnaik, A.R., 1996, in Astrophysical Applications of Gravitational Lensing, IAU 173, ed. C.S. Kochanek, & J. N. Hewitt (Dordrecht: Kluwer) 191

Kneib, J.P., & Soucail, G., 1996, in Astrophysical Applications of Gravitational Lensing, IAU 173, ed. C.S. Kochanek, & J. N. Hewitt (Dordrecht: Kluwer) 113

Kochanek, C.S., 1991a, ApJ, 373, 354

Kochanek, C.S., 1991b, ApJ, 379, 517

Kochanek, C.S., 1993, ApJ, 419, 12

Kochanek, C.S., 1994, ApJ, 436, 56

Kochanek, C.S., 1995a, ApJ, 445, 559

Kochanek, C.S., 1995b, ApJ, 453, 545

Kochanek, C.S., 1996a, ApJ, 466, 638

Kochanek, C.S., 1996b, *ApJ, in press.*

Kochanek, C.S., & Apostolakis, J. 1988, MNRAS, 235, 1073

Kochanek, C.S., & Blandford, R.D. 1987, ApJ, 321, 676

Kochanek, C.S., Falco, E.E., & Schild, R., 1995, ApJ, 452, 109

Kormann, R., Schneider, P., & Bartelmann, M., 1994a, A&A, 284, 285

Kormann, R., Schneider, P., & Bartelmann, M., 1994b, A&A, 286, 357

Kovner, I. 1987, ApJ, 316, 52

Lawrence, C.R., Schneider, D.P., Schmidt, M., Bennett, C.L., Hewitt, J.N., Burke, B.F., Turner, E.L., & Gunn, J.E., 1984, Science, 223, 46

Loveday, J., Peterson, B.A., Efstathiou, G., & Maddox, S.J., 1992, ApJ, 390, 338

Maoz, D., & Rix, H.-W. 1993, ApJ, 416, 425

Maoz, D., Bahcall, J.N., Doxsey, R., Schneider, D.P., Bahcall, N.A., Lahav, O., & Yanny, B., 1993a, ApJ, 402, 69

Maoz, D., Bahcall, J.N., Schneider, D.P., Bahcall, N.A., Lahav, O., Djorgovski, S., Doxsey, R., Gould, A., Kirhakos, S., & Yanny, B., 1993b, ApJ, 409, 28

Marzke, R.O., Geller, M.J., Huchra, J.P., & Corwin, H.G., 1994, AJ, 108, 437

Miralda-Escudé, J. 1991, ApJ, 380, 1

Mould, J., Blandford, R., Villumsen, J., Brainerd, T., Smail, I., Small, T., & Kells, W., 1994, MNRAS, 271, 31

Myers, S.T., Fassnacht, C.D., Djorgovski, S.G., et al., 1995, ApJ, 447, L5

Myers, S.T., 1996, in Astrophysical Applications of Gravitational Lensing, eds., C.S. Kochanek & J.N. Hewitt (Kluwer: Dordrecht) 317

Nair, S., & Garrett, M.A., 1996, in Astrophysical Applications of Gravitational Lensing, IAU 173, eds. C.S. Kochanek, & J. N. Hewitt (Dordrecht: Kluwer) 197

Patnaik, A.R., 1994, in Gravitational Lenses in the Universe, eds., J. Surdej, D. Fraipont-Caro, E. Gosset, S. Refsdal, & M. Remy (Liège, Université de Liège) 311

Patnaik, A.R., Browne, I.W.A., King, L.J., Muxlow, T.W.B., Walsh, D., & Wilkinson, P.N., 1992, in Gravitational Lenses, ed. R. Kayser, T. Schramm, & L. Nieser (Springer: Berlin) 140

Peacock, J.A., & Dodds, S.J. 1996, MNRAS, 280, 19

Postman, M., & Geller, M.J., 1984, ApJ, 281, 95

Ratnatunga, K.U., Ostrander, E.J., Griffiths, R.E., & Im, M., 1995, ApJ, 453, L5

Rybicki, G.B, 1987, in Structure and Dynamics of Elliptical Galaxies, IAU Symp. 127, eds. T. de Zeeuw (Dordredcht: Kluwer), 397

Ryden, B.S. 1992, ApJ, 396, 445

Sackett, P.D., Rix, H.-W., Jarvis, B.J., & Freeman, K.C., 1994, ApJ, 436, 629

Saglia, R.P., et al., 1993, ApJ, 403, 567

Schechter, P., 1976, ApJ, 203, 297

Schechter, P., 1987, in Structure and Dynamics of Elliptical Galaxies, IAU Symp. 127, eds. T. de Zeeuw (Dordredcht: Kluwer), 217

Schechter, P., et al., 1996, *preprint preprint*

Seljak U. 1994, ApJ, 436, 509

Seljak U. 1996, ApJ, 463, 1

Subramanian, K., & Cowling, S.A., 1986, MNRAS, 219, 333

Surdej, J., Claeskens, J.F., Crampton, D., Filippenko, A.V., Hutsemékers, D., Magain, P., Pirenne, B., Vanderriest, C., & Yee, H.K.C., 1993, AJ, 105, 2064

Turner, E.L., 1990, ApJ, 365, L43

Turner, E.L., Ostriker, J.P., & Gott, J.R. 1984, ApJ, 284, 1

Valdes, F., Jarvis, J.F., Mills, A.P., & Tyson, J.A., 1984, ApJ, 281, L59

Wallington, S., & Narayan, R., 1993, ApJ, 403, 517

Walsh, D., Carswell, R.F., Weymann, R.J. 1979, Nature, 279, 381

Wambsganss, J., & Paczyń ski, B. 1994, AJ, 108, 1156

Wambsganss, J., Cen, R., Ostriker, J.P., & Turner, E.L., 1995, Science, 268, 274

Warren, M.S., Quinn, P.J., Salmon, J.K., & Zurek, W.H. 1992, ApJ, 399, 405

Yee, H.K.C., Fillipenko, A.V., & Tang, D., 1993, AJ, 105, 7

Young, P., Gunn, J.E., Oke, J.B., Westphal, J.A. & Kristian, J., 1980, ApJ, 241, 507

Young, P., Deverill, R.S., Gunn, J.E., & Kristian, J., 1981, ApJ, 244, 723